Lithos 126 (2011) 321–340

Contents lists available at ScienceDirect

Lithos

journal homepage: www.elsevier.com/locate/lithos

Geochemical and geochronological studies of granitoid rocks from the Western Tianshan Orogen: Implications for continental growth in the southwestern Central Asian Orogenic Belt

Lingli Long [a,b,c], Jun Gao [a,b,*], Reiner Klemd [d], Christoph Beier [d], Qing Qian [b], Xi Zhang [a,b], Jingbin Wang [c], Tuo Jiang [b]

[a] Xinjiang Research Centre for Mineral Resources, Xinjiang Institute of Ecology and Geography, Chinese Academy of Sciences, Urumqi 830011, China
[b] Key Laboratory of Mineral Resources, Institute of Geology and Geophysics, Chinese Academy of Sciences, PO Box 9825, Beijing 100029, China
[c] Beijing Institute of Geology for Mineral Resources, Beijing 100012, China
[d] GeoZentrum Nordbayern, Universität Erlangen-Nürnberg, Schlossgarten 5a, 91054 Erlangen, Germany

ARTICLE INFO

Article history:
Received 18 January 2011
Accepted 23 July 2011
Available online xxxx

Keywords:
Granitoid rocks
Zircon U–Pb age
Sr–Nd isotope
Continental growth
Tianshan

ABSTRACT

The Western Tianshan Orogen in northwestern China is part of the southwestern margin of the Central Asian Orogenic Belt (CAOB), which represents the largest tectonic assembly of accretionary complexes and the most significant area of Phanerozoic continental growth in the world. Granitoid rocks have a widespread occurrence and occupy about 30% of the whole exposure of the orogen. Ages obtained for the granitoids vary from 896 Ma to 247 Ma, while initial $^{87}Sr/^{86}Sr$ ratios vary from 0.70329 to 0.72070 and ε_{Nd} values from −14.1 to +7.3. The occurrence of Neoproterozoic granitic gneisses implies the presence of Precambrian basement in this area. During oceanic subduction, continental growth occurred as a result of several combined processes, i.e. by addition of oceanic crustal melts (adakites), the intrusion of basaltic magmas derived by partial melting of the metasomatized depleted mantle wedge and the upwelling of granitic magma derived from a mixed source of basaltic magmas and old continental basement. However, during the post-collisional period, vertical accretion of underplated juvenile mantle material may have been accomplished during 'slab breakoff' delamination. This study suggests a two stage model of continental growth of 'syn-subduction lateral accretion of arc complexes' and 'post-collisional vertical accretion of underplated mantle material', which may also be relevant for the western segment of the CAOB in the Phanerozoic. The reworking and involvement of old crust are more obvious in the Western Tianshan Orogen compared to other parts of the CAOB comprising the Western Junggar, Eastern Junggar, Alataw and Altay terranes.

1. Introduction

The Central Asian Orogenic Belt (CAOB) also known as the 'Altaid tectonic collage' is one of the world's largest accretionary orogens. Nearly half of the newly formed continental crust of the CAOB was formed by arc accretion in the Phanerozoic (Sengör et al., 1993). Systematic geochemical and geochronological studies on granitoids in the Junggar and Alataw terranes of NW China contrastingly indicate that the granitoids with positive εNd and low-Sr isotopic ratios were derived from a long-lived depleted mantle reservoir in a post-collisional environment (Chen and Arakawa, 2005; Chen et al., 2000a; Han et al., 1997, 2006). The granitoids in the Altay (Sun et al., 2008; Wang et al., 2006a, 2009a; Yuan et al., 2007), Mongolia (Jahn et al., 2004; Kröner et al., 2007), central Kazakhstan (Heinhorst et al., 2000), central and northern Kazakhstan terranes (Kröner et al., 2008) were predominantly generated in subduction zone settings indicating lateral continental growth by accretion of arc complexes (Jahn, 2004; Jahn et al., 2000). Furthermore, Permian anorogenic, rift-related alkaline granite magmatism occurs locally in central and northern Kazakhstan reflecting vertical addition of juvenile, mantle-derived material by underplating (Heinhorst et al., 2000; Kröner et al., 2008).

Therefore, two different models aim to explain the mechanism of the Phanerozoic continental growth in the CAOB: the 'syn-subduction continental growth by accretion of arc complexes related to oceanic subduction' (Sengör et al., 1993; Xiao et al., 2009a, 2009b) and the 'syn-subduction lateral continental growth by accretion of arc complexes as well as post-collisional vertical continental growth by accretion of mantle-derived material' (Han et al., 1997; Jahn et al., 2000; Wang et al., 2009a).

Granitoids can be used as tracers of the geodynamic evolution (e.g., Barbarin, 1999) and the continental growth process of orogens (e.g., Han et al., 1997; Wang et al., 2009a). Compared with granitoids in other parts of the CAOB, the isotopic characteristics and ages of

* Corresponding author at: Key Laboratory of Mineral Resources, Institute of Geology and Geophysics, Chinese Academy of Sciences, PO Box 9825, Beijing 100029, China.
E-mail addresses: gaojun@mail.igcas.ac.cn (J. Gao), klemd@geol.uni-erlangen.de (R. Klemd).

0024-4937/$ – see front matter © 2011 Elsevier B.V. All rights reserved.
doi:10.1016/j.lithos.2011.07.015

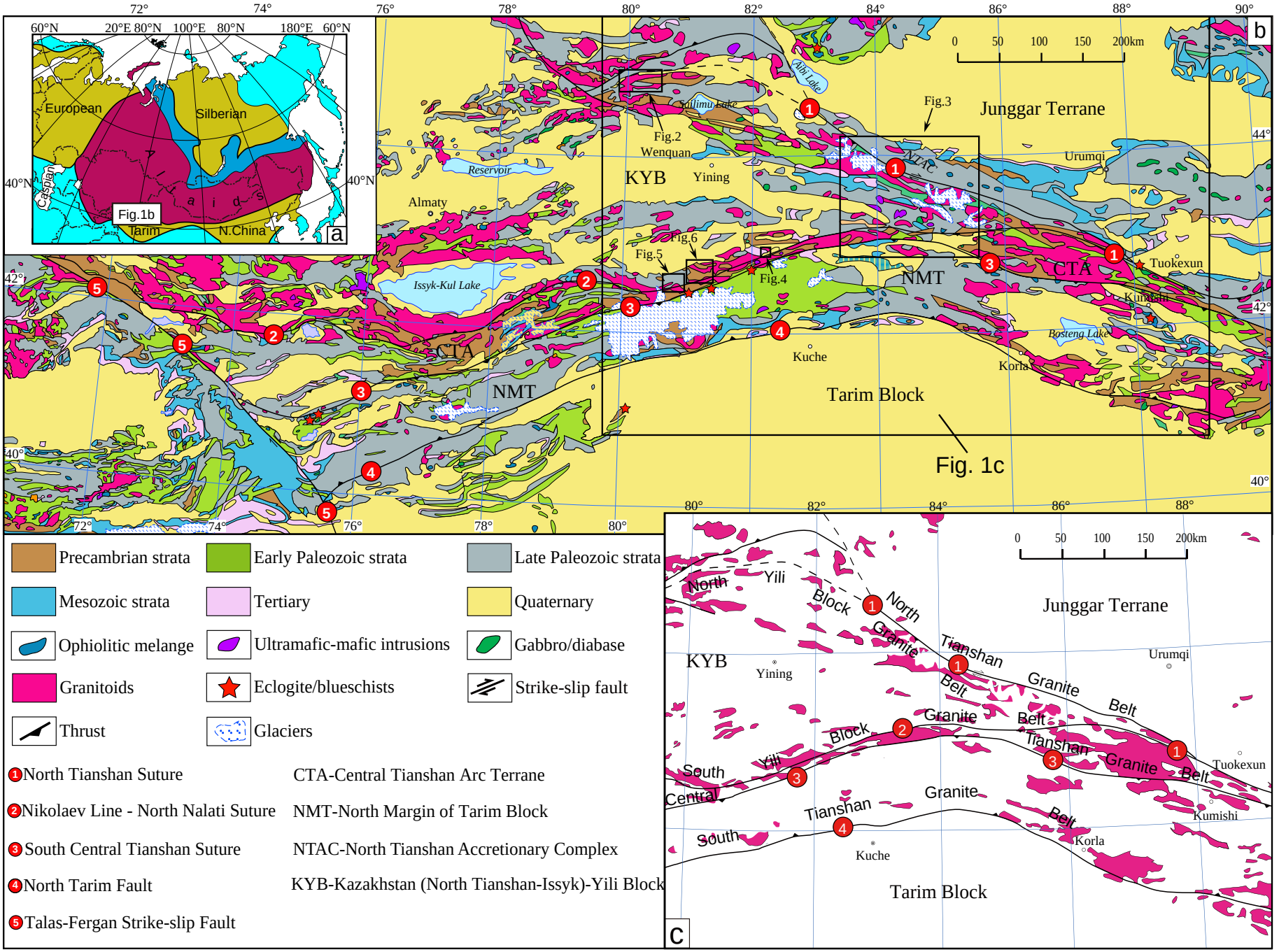
a
European
Siberian
Tarim
N.China
Caspian
Fig.1b
b
Junggar Terrane
Fig.3
Fig.2
Wenquan
Yining
KYB
Almaty
Reservoir
Issyk-Kul Lake
Fig.6
Fig.5
Fig.4
CTA
NMT
NTAC
Urumqi
Tuokexun
Kumishi
Bosteng Lake
Kuche
Korla
Tarim Block
Fig. 1c
Precambrian strata
Early Paleozoic strata
Late Paleozoic strata
Mesozoic strata
Tertiary
Quaternary
Ophiolitic melange
Ultramafic-mafic intrusions
Gabbro/diabase
Granitoids
Eclogite/blueschists
Strike-slip fault
Thrust
Glaciers
1 North Tianshan Suture
2 Nikolaev Line - North Nalati Suture
3 South Central Tianshan Suture
4 North Tarim Fault
5 Talas-Fergan Strike-slip Fault
CTA-Central Tianshan Arc Terrane
NMT-North Margin of Tarim Block
NTAC-North Tianshan Accretionary Complex
KYB-Kazakhstan (North Tianshan-Issyk)-Yili Block
c
Yili Block
North Tianshan Granite Belt
South Central Tianshan Granite Belt
Junggar Terrane
Yining
KYB
Urumqi
Tuokexun
Kumishi
Kuche
Korla
Tarim Block

rocks exposed in the Tianshan Orogen, which occupies the southwest margin of the CAOB (Fig. 1a), have not yet been studied systematically.

Here, we present Laser-Ablation ICP-MS trace element data (LA-ICP-MS) and SHRIMP U–Pb zircon age data from 13 representative plutons and, in addition, strontium and neodymium isotopic data from 15 plutons. We develop a model, together with published data (95 zircon U–Pb ages and 92 Sr–Nd isotopic ratios) to elucidate the Phanerozoic continental growth in the Western Tianshan Orogen. These data show that continental growth in the Western Tianshan occurred as a result of syn-subduction lateral accretion of arc complexes and post-collisional vertical accretion and thus by combining the two models proposed for continental growth in the western segment of the CAOB.

2. Regional geology and distribution of granitoid rocks

The Chinese Western Tianshan orogen and adjacent regions are subdivided into four distinct tectonic domains: the Northern Tianshan Accretionary Complex, the Kazakhstan (North Tien Shan–Issyk-Kul)–Yili block, the Central Tianshan Arc Terrane and the Tarim block. These are separated by the North Tianshan (or Northern Central Tianshan), the Nikolaev Line-North Nalati and the South Central Tianshan (or South Tianshan) suture zones, respectively (Fig. 1b; Gao et al., 2009; Qian et al., 2009). The North Tianshan suture zone was suggested to have formed during the late Carboniferous (Han et al., 2010a; Wang et al., 2006b). The activity of the Nikolaev Line-North Nalati suture zone terminated at the end of Middle Ordovician (Bazhenov et al., 2003), while the timing of the activity of the South Central Tianshan suture zone is still controversial (e.g., Hegner et al., 2010). The latter has traditionally been regarded as a Late Paleozoic major shear zone between the Tarim and Yili-(Central Tianshan) blocks (e.g., Allen et al., 1992; Charvet et al., 2007; Gao et al., 2011), while Xiao et al. (2009a, 2009b) and Zhang et al. (2007) concluded recently that this suture zone formed during the Triassic.

Granitoid rocks have a widespread occurrence in the Western Tianshan Orogen and mark the main period of continental growth of northwestern China (Coleman, 1989). They occupy about 30% of the whole orogen (Wang et al., 1990). The distribution of these granitoids is restricted to five belts: the North Tianshan Granite Belt, the North Yili Block Granite Belt, the South Yili Block Granite Belt, the Central Tianshan Granite Belt, and the South Tianshan Granite Belt (Fig. 1c; Han et al., 2010a); Long, 2007; Wang et al., 1990; Xiao et al., 1992.

The North Tianshan Granite Belt (NTGB) consists of several granitic plutons, which are intruding into the North Tianshan accretionary complex (Fig. 1c; Han et al., 2010a; Wang et al., 2006b). The accretionary complex is mainly composed of Devonian–Carboniferous turbidites and volcanosedimentary rocks and ophiolite remnants of the Junggar (or North Tianshan) oceanic crust (Gao et al., 1998; Wang et al., 2006b). Late Carboniferous continental conglomerates that occur in few local outcrops lie above a discontinuity on top of the volcanics of the accretionary complex (Wang et al., 1994). The Kikeshu pluton crops out in an area of ~200 km^2 and intruded into the ophiolitic mélange interpreted as a post-collisional stitching intrusion with SHRIMP zircon U–Pb ages of 316 ± 3 Ma (Han et al., 2010a).

The North Yili Block Granite Belt (NYBG) extends for more than 400 km along the northern margin of the Yili block bordered by the Late Paleozoic North Tianshan suture zone to the north and the Yili basin to the south (Fig. 1c). The granitoids intruded into Meso–Neoproterozoic gneisses and sediments, Cambrian–Early Ordovician and Silurian sediments. Furthermore, they intimately occur together with Early Carboniferous basaltic to intermediate volcanics (Gao et al., 1998; Wang et al., 2007; Zhai et al., 2009). SHRIMP, Laser-Ablation ICP-MS and TIMS U–Pb zircon ages range from 390 Ma to 287 Ma for the granitoids (Li et al., 2006; Tang et al., 2007, 2010a; Wang et al., 2006b; Xu et al., 2006; Zhang et al., 2008, 2010a; Zhu et al., 2006a). Late Ordovician amphibolites with U–Pb zircon ages of 455 and 451 Ma are exposed in the Wenquan area (Fig. 1b) which was formerly interpreted to represent the Precambrian basement (Hu et al., 2008).

The South Yili Block Granite Belt (SYGB; Fig. 1c) stretches from the southern margin of the Yili block in China to the Northern Tianshan of Kyrgyzstan and Kazakhstan. Meso- to Neoproterozoic low-grade metamorphic clastic rocks, Sinian (latest Neo-Proterozoic) tillites and Cambrian transitional Mid-Ocean Ridge Basalts (T-MORB; 516 ± 7 Ma, SHRIMP zircon U–Pb age) are locally exposed in the Chinese part of the SYGB (Qian et al., 2009). In addition, diorites (470 ± 12 Ma, SHRIMP zircon U–Pb age) intruded into the Cambrian volcanic rocks (Qian et al., 2009). Early Carboniferous andesites, basaltic andesites and basalts with $^{40}Ar/^{39}Ar$ ages of 334–360 Ma (Liu et al., 1994) and a SHRIMP zircon U–Pb age of 361 ± 6 Ma (Zhu et al., 2009) and Late Carboniferous–Early Permian alkali-rich volcanic rocks (Fig. 1b; Zhao et al., 2009) are distributed along the Chinese part of the granite belt. Adakitic quartz-albite porphyries and dacites with a SHRIMP zircon U–Pb age of 259.5 ± 0.5 Ma have also been reported to occur as small plutons in the Awulaleshan of the SYGB (Zhao et al., 2008). In southern Kazakhstan, Archean granitic SYGB gneisses have SHRIMP zircon U–Pb ages of 2791.0 ± 24 Ma and Paleoproterozoic granitic gneisses have ages of 2187.1 ± 0.5 and 1789.1 ± 0.6 Ma (Kröner et al., 2007). Furthermore, the Precambrian basement was overthrust by Cambrian to Lower Arenigian (earliest Early Ordovician) ocean island and island arc complexes that are unconformably overlain by Middle Arenigian conglomerates and olistostromes (Mikolaichuk et al., 1997). Precambrian to Middle Ordovician rocks were intruded by granites in the middle Ordovician (460–470 Ma, U–Pb zircon age, Konopelko et al., 2008) and Early Silurian (435–440 Ma, U–Pb zircon age, Konopelko et al., 2008). Upper Arenigian to Lower Caradocian island arc volcanic rocks and Upper Ordovician redbeds are unconformably covered by Devonian volcanics, Lower Carboniferous redbeds, Upper Carboniferous conglomerates and sandstones (Mikolaichuk et al., 1997). Additionally, Permian alkali-rich volcanic rocks including shoshonites unconformably overlie Upper Carboniferous sedimentary rocks in Northern Tianshan of Kyrgyzstan and Kazakhstan (Solomovich, 2007).

The narrow Central Tianshan Granite Belt (CTGB) is framed by the Early Paleozoic Nikolaev Line-North Nalati suture to the north and the Late Paleozoic South-Central-Tianshan suture to the south (Fig. 1c). It is underlain by Meso- to Neoproterozoic metamorphic basement, which is composed of sillimanite–biotite–quartz schists, garnet–plagioclase–granulites, gneisses, amphibolites, migmatites and marbles (Wang et al., 1990; Xiao et al., 1992). The basement itself lies under a disconformity of Sinian carbonates and tillites. Late Silurian and Carboniferous island–arc volcanic and volcaniclastic rocks were thrust over the Precambrian metamorphic rocks (Gao et al., 1998; Zhu et al., 2005, 2009). Late Permian sediments are present locally. Early Paleozoic to Late Paleozoic diorites and granites with zircon U–Pb ages varying from 479 Ma to 266 Ma (Gao et al., 2009; Han et al., 2004; Li et al., 2010; Yang et al., 2006; Zhu et al., 2006b) intruded into the Meso- to Neoproterozoic metamorphic basement, Late Silurian and Carboniferous island–arc type volcanics.

Few granitic plutons of the South Tianshan Granite Belt (STGB; Fig. 1c) intruded into the northern margin of the Tarim block predominantly composed of Proterozoic metamorphic rocks, Sinian and Lower Cambrian sediments and Cambrian–Carboniferous marine/non-marine carbonates, clastic rocks, cherts and interlayered volcanics (Carroll et al., 1995). Permian fluvial deposits and rift-type

Fig. 1. Tectonic map of the Western Tianshan Orogen (a) modified after Zhang et al., 2010a; b) modified after Gao et al., 2009) showing the distribution of Paleozoic granitic rocks (c, modified after Wang et al., 1990). Maps in Figs. 2, 3, 4, 5 and 6 are outlined.

volcanics unconformably lie underneath the earlier strata locally. Granitic plutons are predominantly composed of syenites, nepheline syenites, aegirine syenites, two-mica peraluminous leucogranites and A-type rapakivi granites, which revealed U–Pb zircon ages of 304–273 Ma (Konopelko et al., 2007; Liu et al., 2004; Long et al., 2008; Seltmann et al., 2011; Solomovich, 2007; Zhu et al., 2008a). Several granitic intrusions containing zircon grains with ages from 490 Ma to 387 Ma occur in the eastern segment of the STGB (Han et al., 2004; Hopson et al., 1989; Zhu et al., 2008b).

3. Localities and description of samples

Granitoids from 13 granitic plutons from the NYGB, the SYGB, the CTGB and the STGB have been selected for age dating (Table 1). These plutons and nine other granitic intrusions that were previously dated (see below and Gao et al., 2009) have been selected for major element and trace element analyses. Fifteen of them have been selected for Sr–Nd isotope analyses.

3.1. The North Yili Block Granite Belt (NYGB)

The western segment of the NYGB contains a composite granitic pluton of biotite monzo-diorite, granodiorite, diorite and granite that is exposed in the Wenquan region (Fig. 1b). It intrudes into the Paleo- and Meso-Proterozoic Wenquan Group and Devonian strata (Fig. 2). The Wenquan Group mainly consists of migmatitic gneisses, granitic gneisses, biotite–quartz schists and marbles. The Devonian strata are composed of siltstones, sandstones, conglomerates, limestones and minor interlayered tuffs. The granitic sample WQ2 selected for dating displays a massive texture and consists of biotite (20%), alkaline feldspar (25%), plagioclase (30%), quartz (24%) and accessory minerals such as zircon, apatite, ilmenite and magnetite.

Another composite granitic intrusion which is composed of biotite diorite, biotite granodiorite and hornblende biotite granite is exposed along the Du–Ku High Road across the eastern segment of the NYGB (Figs. 1b and 3). It intruded into Silurian or Carboniferous sedimentary and volcanic rocks (Fig. 3; Wang et al., 2006b, 2007). The biotite granodiorite displays a mylonitic foliation that is parallel to the trend of the North Tianshan suture zone and dips to the south. The surrounding biotite diorite and hornblende–biotite granite are massive in character. Sample DK 14 is composed of biotite (20%), plagioclase (55%), alkaline feldspar (5%), quartz (20%) and minor accessory minerals such as zircon, apatite, ilmenite and magnetite. The biotite diorite (sample DK11) and the hornblende–biotite granite (sample DK13) contain 25% and 1% hornblende, respectively. The quartz content of the biotite granodiorite is 3% and the biotite diorite contains about 20% quartz.

3.2. The South Yili Block Granite Belt (SYGB)

The alkali feldspar granite intrusion selected for this study is exposed along the Qiongkushitai River across a narrow corridor between the Early Paleozoic North Nalati suture and the Late Paleozoic South Central Tianshan suture (Figs. 1b and 4). The alkali feldspar granite pluton is thrust over Early Carboniferous volcanic and volcaniclastic rocks. The investigated sample QK7 consists of alkali feldspar (60%), plagioclase (10%), quartz (29%), minor biotite (1%) and accessory minerals.

3.3. The Central Tianshan Granite Belt (CTGB)

The Central Tianshan Arc Terrane that crops out along the Muzaerte River (Figs. 1b and 5) consists of a hornblende granodioritic intrusion overlain by Carboniferous volcanic rocks and limestones. A biotite–hornblende granodiorite pluton intruded into amphibolite-facies schists, granulites, gneisses and amphibolites. The hornblende granodiorite (samples XT5/14/16/17) has a coarse-grained massive texture and is mainly composed of alkali feldspar (20%–40%), plagioclase (20%–30%), quartz (20%–35%) and hornblende (10%–15%). The biotite–hornblende granodiorite (sample XT18/19) displays a weak gneissic foliation, which is parallel to the main ENE regional

Table 1
The descriptional data on geology, geochemistry and geochronology for the intrusions in this study.

Intrusion (sample)	Rock type	Tectonic setting	Country rocks	Age (Ma)	Geochemistry of major elements	Geochemistry of trace elements	Initial $^{87}Sr/^{86}Sr$	εNd(T)
WQ2	Biotite monzo-diorite	NYGB	Meso-Proterozoic and Devonian strata	371.3 ± 1.5	δ: 1.32 to 2 A/CNK: 0.99 to 1.09 Fe*: 0.84 to 0.86	LREE-Enrichment, flat HREEs Negative anomalies for Ba, Nb, Ta, Sr and Ti	0.713496	−2.61
DK11	Biotite diorite	NYGB	Carboniferous strata	281.2 ± 1.2	δ = 1.94,A/CNK = 0.69, Fe* = −5.2	LREE-Enrichment, Flat HREEs	–	–
DK13	Biotite granite	NYGB	Carboniferous strata	296.6 ± 0.8	δ = 2.28,A/CNK = 1, Fe* = 0.8	Less depletion of Nb and Ta		
DK14	Biotite granodiorite	NYGB	Silurian strata	412.6 ± 2.4	δ = 0.83,A/CNK = 1.15, Fe* = 0.66	LREE-Enrichment, flat HREEs Depletion of Ba, Nb, Ta, Sr and Ti	– –	– –
QK7	Alkali feldspar granite	SYGB	Thrust over Carboniferous strata	430 ± 8	δ = 1.88,A/CNK = 1.21, Fe* = 0.84	LREE-Enrichment, Flat HREEs Depletion of Ba, Nb, Ta, Sr and Ti	–	–
XT17	Hornblende granodiorite	CTGB	Thrust over Carboniferous strata	437.4 ± 1.1	δ = 2.19,A/CNK = 0.98, Fe* = 0.71	LREE-Enrichment, Flat HREEs Depletion of Ba, Nb, Ta, Sr and Ti	0.716343	−6.50
XT18	Hornblende granodiorite	CTGB	Precambrian strata	247.2 ± 0.9	δ = 1.83,A/CNK = 0.93, Fe* = 0.73	LREE-Enrichment, Flat HREEs Without Nb and Ta anomalies	–	–
AK8	Diorite	CTGB	Precambrian strata	409.0 ± 1.6	δ = 4.36,A/CNK = 0.92, Fe* = 0.74	LREE-Enrichment, Flat HREEs Depletion of Ba, Nb, Ta, Sr and Ti	0.709989	−0.79
QK1	Monzodiorite	CTGB	Precambrian and Late Paleozoic strata	325 ± 5	δ = 2.64,A/CNK = 0.66, Fe* = 0.64	LREE-Enrichment, Flat HREEs Without Nb and Ta anomalies	0.706829	−0.84
QK5	Biotite granite	CTGB	Precambrian and Late Paleozoic strata	322 ± 5	δ = 1.30,A/CNK = 0.94, Fe* = 0.75	LREE-Enrichment, Flat HREEs Without Nb and Ta anomalies	0.707190	−0.87
DK24	Granitic mylonites	CTGB	Precambrian strata	341.5 ± 0.9	δ = 1.90,A/CNK = 0.96, Fe* = 0.71	–	–	–
DK29	Biotite diorite	CTGB	Precambrian strata	320.8 ± 1.1	δ = 3.65,A/CNK = 0.77, Fe* = 0.80	LREE-Enrichment, Flat HREEs Depletion of Ba, Nb, Ta, Sr and Ti	–	–
DK28	Granitic gneiss	CTGB	Precambrian strata	895.6 ± 2.4	δ = 1.43,A/CNK = 1.12, Fe* = 0.81	LREE-Enrichment, Flat HREEs Depletion of Ba, Nb, Ta, Sr and Ti	–	–

Note: NYGB = North Yili Block Granite Belt, SYGB = South Yili Block Granite Belt, CTGB = Central Tianshan Granite Belt; δ = (Na2O + K2O)2/(SiO2-43), A/CNK [molar Al2O3/[CaO + Na2O + K2O]], Fe* [FeOtotal/(FeOtotal + MgO)];"–" = without data.

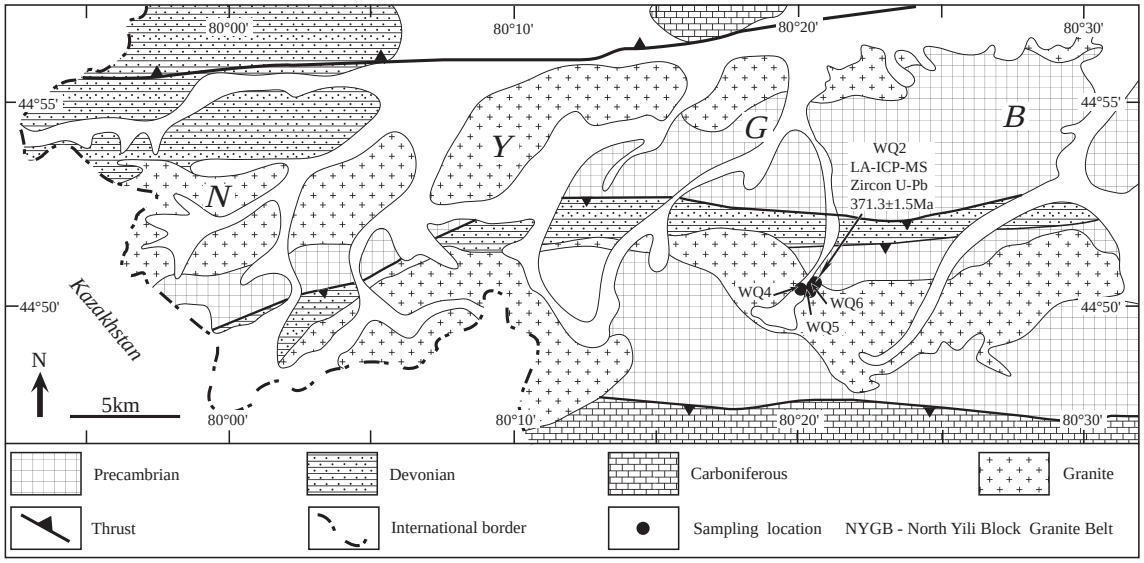

Fig. 2. Geological map of the Western segment of the North Yili Block Granite Belt.

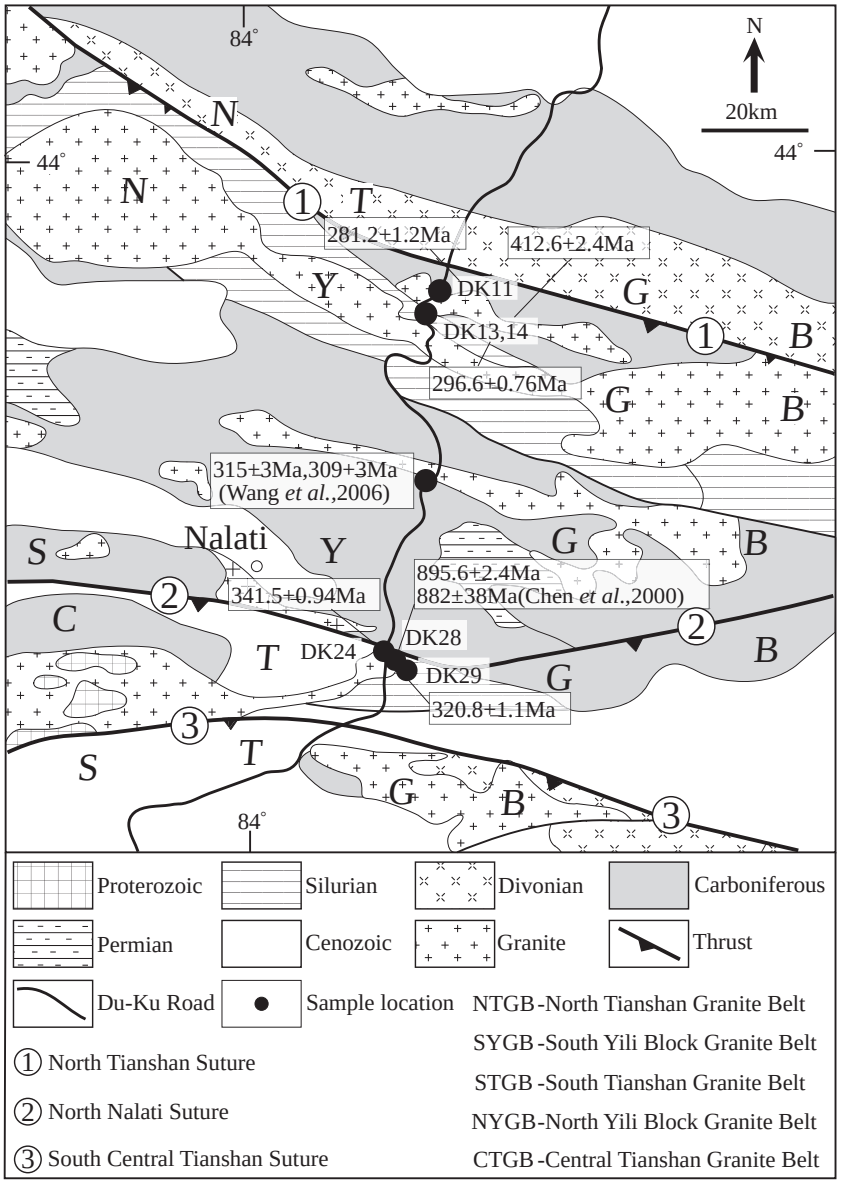

Fig. 3. Geological map of the northern segment of the Du–Ku High Road. The ages were obtained by LA-ICP-MS zircon U–Pb analyses.

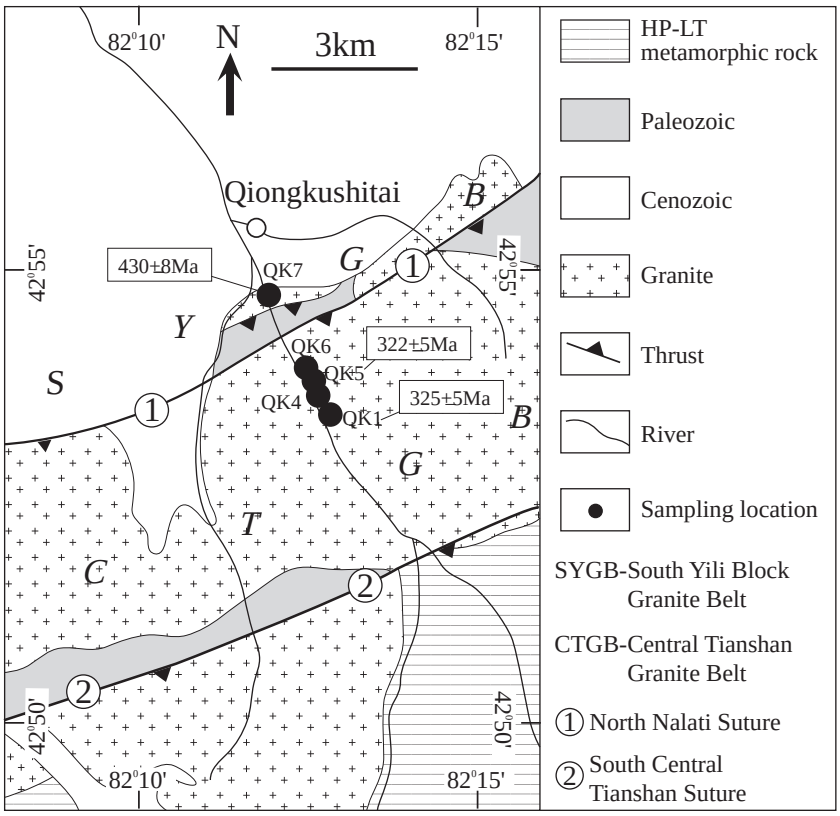

Fig. 4. Geological map along the Qiongkushitai River. The ages were obtained using SHRIMP zircon U–Pb analyses.

trend and consists of alkali feldspar (25%–45%), plagioclase (10%–30%), quartz (15%–25%), hornblende (10%) and biotite (1%–5%).

A composite granitic intrusion consisting of granite, diorite and granodiorite is exposed along the Akeyazi and Bikai Rivers (Figs. 1b and 6). It intruded into Meso- to Neoproterozoic amphibole–biotite plagioclase schists, garnet–plagioclase granulites, gneisses and amphibolites and is overlain by the Western Tianshan high pressure-low temperature metamorphic belt consisting of blueschist-, eclogite- and greenschist-facies meta-sedimentary rocks and some mafic metavolcanic rocks (Gao and Klemd, 2003; Gao et al., 1999). LA-ICP-MS zircon U–Pb ages for the granodiorites and granites yield 479 ± 2 Ma, 419 ± 2 Ma, 413 ± 1 Ma and 401 ± 1 Ma (samples BK7/14/15/13; Gao et al., 2009). One diorite sample (AK8) containing plagioclase (70%), hornblende (25%), quartz (4%) and ilmenite (1%) was selected for dating and geochemical analyses. Ages and major and trace element composition were also inferred from a hornblende granite (433 ± 6 Ma, sample KKS3), a monzodiorite (398 ± 1 Ma, sample KKS5), a biotite granite (352 ± 5 Ma, sample KKS10), a biotite–hornblende granite (349 ± 6 Ma, sample KKS12) and a quartz syenite (275 ± 3 Ma, sample KKS1) exposed along the Kekesu River (see Fig. 2 of Gao et al., 2009).

A biotite granite and monzodiorite pluton are exposed along the Qiongkushitai River running from south to the north across the Central Tianshan Arc Terrane (Figs. 1b and 4). It intruded into Meso- to Neoproterozoic amphibolite-facies schists, granulites, gneisses and amphibolites and Late Paleozoic blueschist-, and greenschist-facies subduction complexes (Gao et al., 1995). The biotite granite (sample QK5) is composed of biotite (10%), alkali feldspar (50%), plagioclase (20%) and quartz (20%) and the monzodiorite (sample QK1) contains biotite (15%), hornblende (10%), alkali feldspar (35%), plagioclase (30%) and quartz (10%).

Dioritic and granitic plutons intruded into the Meso- and Neoproterozoic amphibolites-facies schists, granulites, gneisses and amphibolites along the Du–Ku High Road (Figs. 1b and 3). The augen gneiss with alkali feldspar porphyroblasts (1–2 cm in diameter) has a foliation parallel to the main ENE regional trend (sample DK28). The gneiss itself is intruded by a biotite diorite (sample DK29) which also intruded into granitic mylonites (sample DK24).

3.4. The South Tianshan Granite Belt (STGB)

A hornblende biotite granite sample from the Heiyingshan area with a SHRIMP zircon U–Pb age of 285 ± 4 Ma (see Fig. 2 of Long et al., 2008) was selected for further Sm–Nd and Rb–Sr isotope studies. It has a gneissic foliation and mainly contains alkali feldspar (~50–65%), plagioclase (<3%), quartz (~25–40%), hornblende (~3–5%) and biotite (5–10%). It is peraluminous and shows a calc-alkaline trend with K_2O/Na_2O ranging from 1.66 to 2.88, $K_2O + Na_2O$ from 7.14 wt.% to 7.79 wt.%, A/CNK value (molar $Al_2O_3/(CaO + Na_2O + K_2O)$) from 0.99 to 1.07 and a δ-value ($\delta = (Na_2O + K_2O)^2/(SiO_2\text{-}43)$) from 1.79 to 2.22 (Long et al., 2008).

4. Results

The detailed analytical methods for the LA-ICPMS and the Sensitive High Resolution Ion Microprobe (SHRIMP) analyses of zircon grains as well as major element, trace element and Sr and Nd isotope compositions of the whole rock powders are described in the 'Analytical methods' in the Supplementary data.

4.1. U–Pb zircon age dating

Zircon grains for U–Pb analyses were separated from thirteen samples (Table 1). Zircon grains are usually elongated or short and prismatic with a length varying from 80 to 250 μm and a width from 45 to 100 μm. They are colorless to light brown, transparent and euhedral with well-developed concentric oscillatory zoning in cathodoluminescence imaging, similar to that of magmatic zircon (Rubatto and

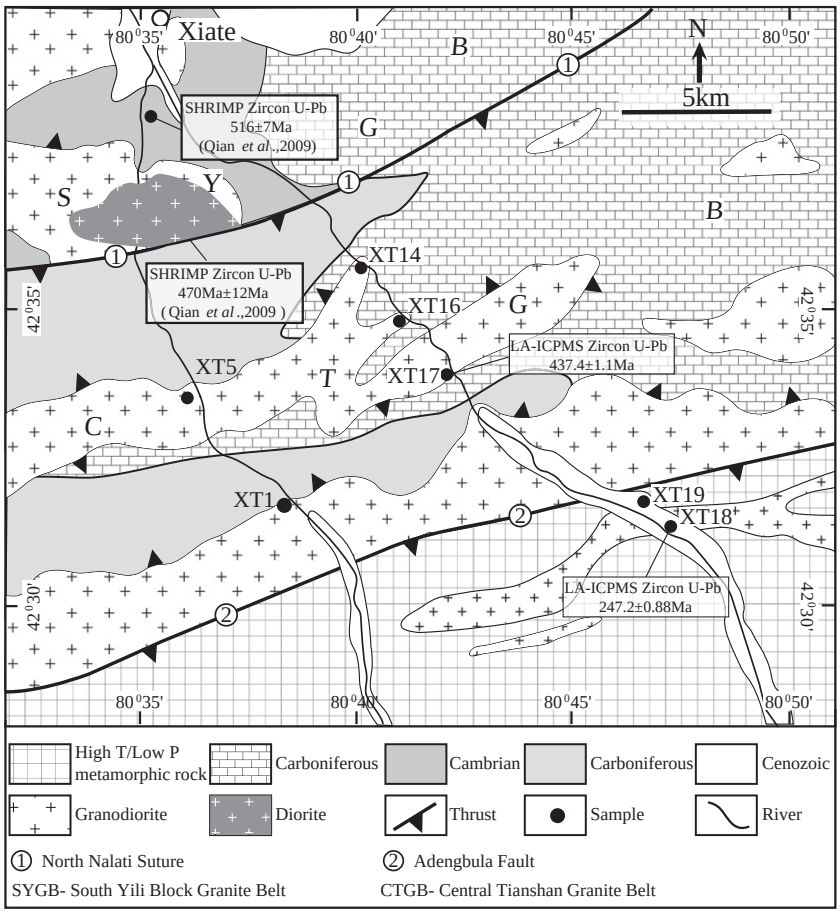

Fig. 5. Geological map along the North Muzaerte River.

Gebauer, 2000). The CL images and analyzed spots of all the studied samples are presented as the Supplementary data. Most analyses were done on zircon rims, some on the mantle domain of zircon grains and few on the core of zircon grains. The results vary within uncertainty for the zircon grains of the same sample. The analytical results for the investigated samples are listed in the Table S1 and Table S2 of the Supplementary data. The U/Th ratio of all analyzed spots varies from 0.1 to 1.42, indicating a magmatic origin for the zircon grains (Williams, 2001). The following geochronological results are presented according to their occurrence in the distinct granite belts.

4.1.1. NYGB

Sixteen zircon analyses from the biotite monzodiorite (sample WQ2) of the western NYGB segment (Fig. 2) have a weighted mean $^{206}Pb/^{238}U$ age of 371.3 ± 1.5 Ma (Fig. 7a). Zircon grains from three samples of the biotite diorite, biotite granodiorite and hornblende–biotite granite exposed in the eastern NYGB segment (Fig. 3) have also been analyzed: four spots analyzed on zircon grains from the biotite granodiorite (sample DK14) are concordant and yield a weighted mean $^{206}Pb/^{238}U$ age of 412.6 ± 2.4 Ma (Fig. 7b). Twenty-one analyses from the biotite diorite (sample DK11) are concordant and give a weighted mean $^{206}Pb/^{238}U$ age of 281.2 ± 1.2 Ma (Fig. 7c). In addition, eighteen zircon analyses from the biotite granite (sample DK13) define a concordant to near-concordant group with a weighted mean $^{206}Pb/^{238}U$ age of 296.6 ± 0.8 Ma (Fig. 7d).

4.1.2. SYGB

Nineteen zircon grains from the alkali feldspar granite exposed along the Qiongkushitai River were analyzed (sample QK7, Fig. 4). Twelve analytical points define a concordant to near-concordant group and give a weighted mean $^{206}Pb/^{238}U$ age of 430 ± 8 Ma (Fig. 7e). The other spots are strongly discordant and were thus excluded from the $^{206}Pb/^{238}U$ age calculation.

4.1.3. CTGB

Thirteen zircon grains from the hornblende granodiorite exposed along the Muzaerte River (sample XT 17, Fig. 5) define a concordant to near-concordant trend with a $^{206}Pb/^{238}U$ age of 437.4 ± 1.1 Ma (Fig. 7f). In addition 15 grains from the biotite–hornblende granodiorite (sample XT 18) exposed ~6 km south of sample XT17 (Fig. 5) are concordant and give a $^{206}Pb/^{238}U$ age of 247.2 ± 0.9 Ma (Fig. 7g).

Thirteen analyses of zircon grains from the diorite exposed along the Akeyazi River (sample AK8; Figs. 6 and 7h) define a concordant age group with a weighted mean $^{206}Pb/^{238}U$ age of 409.0 ± 1.6 Ma. LA-ICP-MS zircon U–Pb ages of 479 ± 2 Ma, 419 ± 2 Ma, 413 ± 1 Ma and 401 ± 1 Ma were reported for the same composite granitoid intrusion (samples BK7/14/15/13; Gao et al., 2009).

Sixteen zircon grains from the monzodiorite exposed along the Qiongkushitai River were analyzed (sample QK1; Fig. 4). Thirteen of which define a concordant to near-concordant weighted mean $^{206}Pb/^{238}U$ age of 325 ± 5 Ma (Fig. 7i). All seventeen analyzed zircon grains of the biotite granite from the same area (sample QK5) yield a weighted mean $^{206}Pb/^{238}U$ age of 322 ± 5 Ma (Fig. 7j).

Eighteen zircon grains from the granitic mylonite exposed at Laerdun Daban along the Du–Ku High Road (sample DK24; Fig. 3) are concordant with a weighted mean $^{206}Pb/^{238}U$ age of 341.5 ± 0.9 Ma (Fig. 7k). Furthermore, 18 spots on zircon grains from the biotite diorite (sample DK29) yield a $^{206}Pb/^{238}U$ age of 320.8 ± 1.1 Ma (Fig. 7l). Thirteen zircon grains from the augen granitic gneiss from the same area, define a concordant to near-concordant trend with a

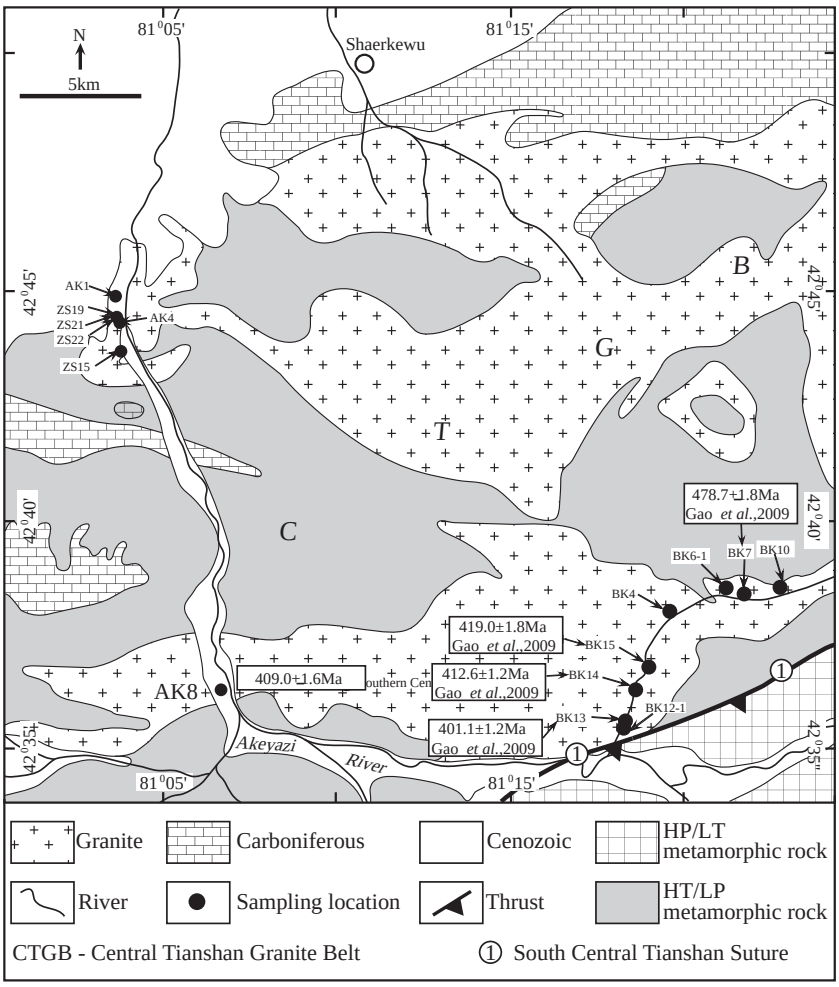

Fig. 6. Geological map along the Akeyazi River. The ages were obtained using LA-ICP-MS zircon U–Pb analyses.

weighted mean $^{206}Pb/^{238}U$ age of 895.6 ± 2.4 Ma (Fig. 7m). This age is within the error range of 882 ± 33 Ma obtained by Chen et al. (1999a) for the same rock types from this locality.

4.2. Geochemical characteristics

Major element, trace element and rare earth element concentrations of granitic rocks are presented in Table S3 of the Supplementary data. Sr–Nd isotope ratios obtained in this study and the data published previously for the granitoids are listed in Table S4 of the Supplementary data. Below, we present the data according to their occurrence in the distinct granite belts.

4.2.1. NYGB

Samples WQ2, WQ4, and WQ6 from the Wenquan area of the western segment of the NYBG are classified as monzodiorite, granodiorite and granite, respectively (Fig. 8a; Middlemost, 1994). They are high potassic calc-alkaline to calc-alkaline rocks with δ-values from 1.32 to 2. They are meta-aluminous to peraluminous with A/CNK between 0.99 and 1.09 while K_2O/Na_2O ratios vary from 1.23 to 1.73. Fe* (FeO^{total} (FeO^{total} + MgO); Frost et al., 2001) (0.84 to 0.86) implies a ferroan, calc-alkaline, peraluminous composition of the biotite monzodiorite.

Generally, samples from the NYGB are characterized by an enrichment of the Light Rare Earth Elements (LREE), flat HREEs and a negative Eu anomaly (with the exception of biotite diorite sample WQ5; Fig. 9a). Chondrite normalized $(La/Yb)_N$ ratios range from 3.03 to 4.72, $(Gd/Yb)_N$ from 1.32 to 1.48 and Eu/Eu* ($=Eu_N/(Sm_N*Gd_N)^{1/2}$) from 0.49 to 0.70. The primitive mantle normalized trace element pattern shows distinct negative anomalies for Ba, Sr, Nb, Ta and Ti (Fig. 9b) and a progressive enrichment of the incompatible elements.

Sample WQ5 from the same pluton is a diorite (Fig. 8a) that has a magnesian, alkaline and metaluminous composition (Fe* = 0.69, δ = 4.24 and A/CNK = 0.69). The REE pattern is comparable to those of samples WQ2, WQ4 and WQ6 but lacks an Eu anomaly and generally has less enriched REE concentrations (Fig. 9a). Its trace element diagram shows slight negative anomalies for Ba, Nb, Ta, Sr and Ti (Fig. 9b). The biotite monzodiorite has a high initial Sr isotope ratio ($(^{87}Sr/^{86}Sr)_i$) of 0.7135, a low $\varepsilon Nd_{(371Ma)}$ value of −2.61 and a Nd model age (T_{DM}) of 1351 Ma (Table S4; Fig. 10).

Three samples (DK11, DK13 and DK14) from the Du–Ku High Road of the eastern segment of the NYGB are diorites, granites and granodiorites (Fig. 8a). The calc-alkaline biotite granodiorite with an age of 412.6 Ma has a magnesian, peraluminous composition (Fe* = 0.66, δ = 0.83 and A/CNK = 1.15). The REE pattern is characterized by a LREE-enrichment, flat HREEs and a negative Eu anomaly (Fig. 9a) while the trace element concentrations display negative anomalies for Ba, Sr, Nb, Ta and Ti and are thus comparable to those of samples of the Wenquan area (Fig. 9b). The hornblende–biotite granite (296.6 Ma) reveals an Fe* of 0.8, a δ of 2.28 and an A/CNK of 1 indicating both

Fig. 7. U–Pb Concordia diagrams showing zircon ages obtained by LA-ICP-MS and SHRIMP. Dashed ellipses show data not included in age calculations because of deviation from the concordant line.

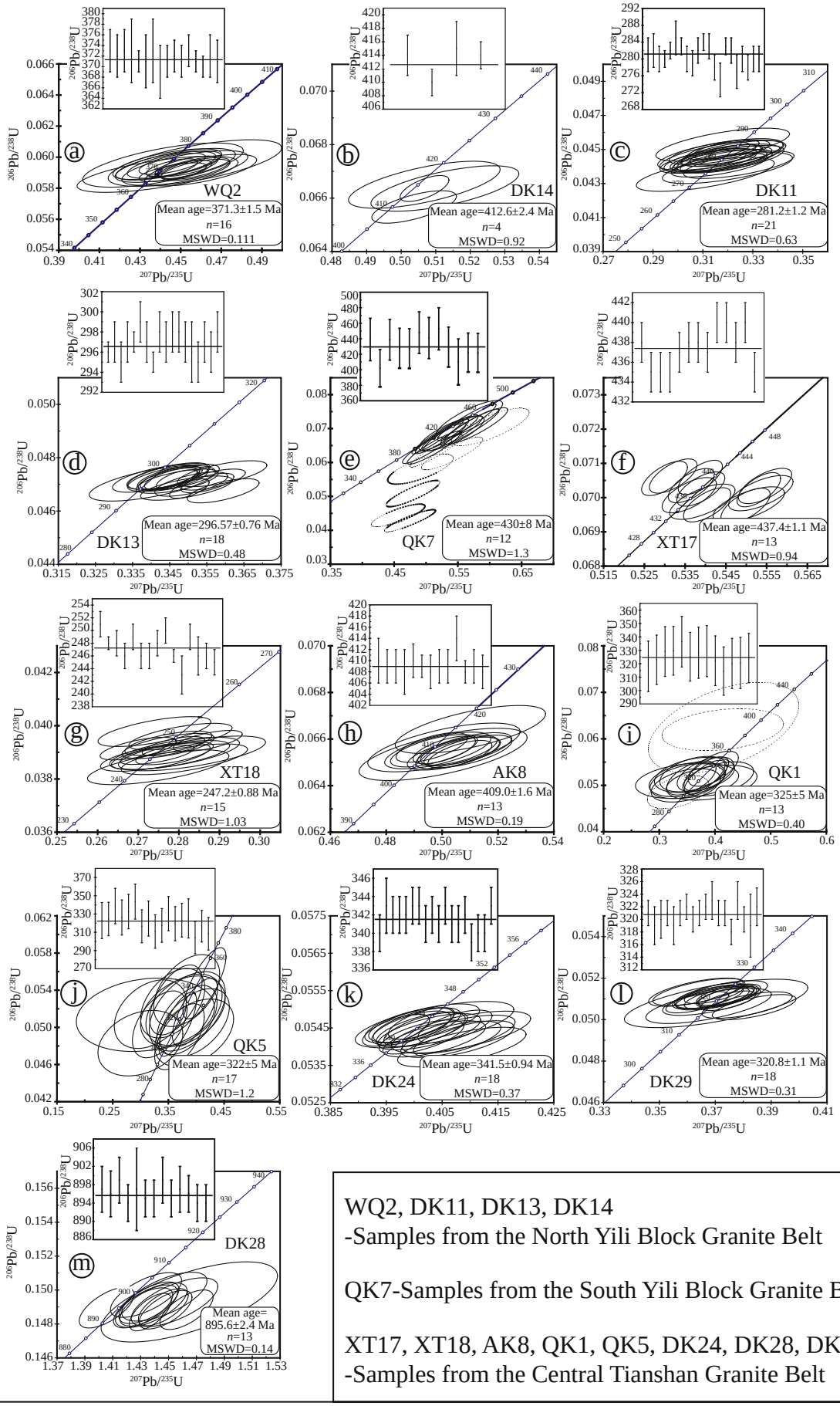

WQ2, DK11, DK13, DK14
-Samples from the North Yili Block Granite Belt

QK7-Samples from the South Yili Block Granite Belt

XT17, XT18, AK8, QK1, QK5, DK24, DK28, DK29
-Samples from the Central Tianshan Granite Belt

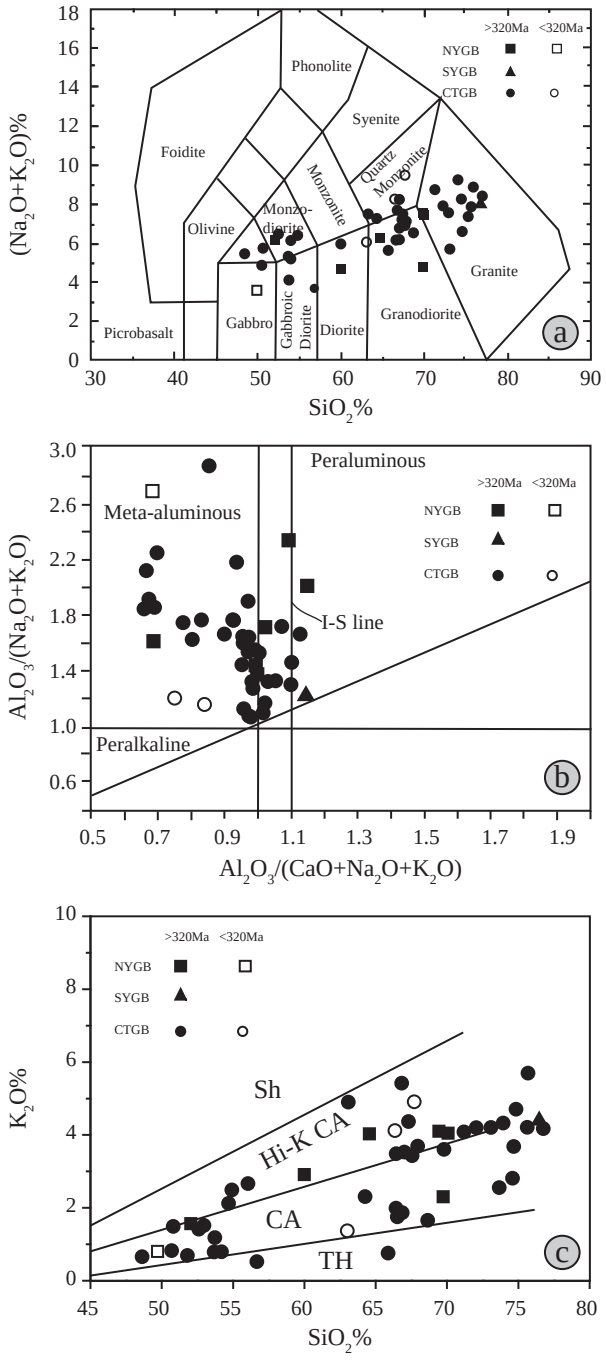

Fig. 8. Major element diagrams for the granitoids. a) TAS classification diagram (after Middlemost, 1994), b) A/NK versus A/CNK diagram of granites (Shand's molar parameters in the diagram after Maniar and Piccoli, 1989), c) K_2O versus SiO_2 diagram (boundaries after Peccerillo and Taylor, 1976). TH: tholeiitic, CA: calc alkaline, Hi–K CA: high potassic calc alkaline, Sh: shoshonitic.

ferro-magnesian and metaluminous–peraluminous and calc-alkaline characteristics. The REE and trace element patterns are similar to those of samples DK11, 13 and 14 (Fig. 9c). The calc-alkaline biotite diorite (281.2 Ma) is magnesian and metaluminous with $Fe^*=0.72$, $\delta=1.94$ and A/CNK = 0.69. The REE pattern is characterized by slight LREE-enrichment, flat HREEs and a slight positive Eu anomaly (Fig. 9c) with $(La/Yb)_N=3.46$, $(Gd/Yb)_N=1.49$ and $Eu/Eu^*=1.29$. Ba, Sr, and Ti anomalies are absent and a potential Nb–Ta trough appears less pronounced (Fig. 9d).

4.2.2. SYGB

The granite intrusion exposed along the Qiongkushitai River (sample QK7) displays a high-K calc-alkaline affinity. The alkali-content ($(K_2O+Na_2O)=7.95$ wt.%, $K_2O/Na_2O=1.21$) and the A/CNK (1.21) indicate the strongly peraluminous character of this granite. It displays a negative Eu anomaly (Eu/Eu* of 0.39), LREE-enrichment and flat HREE-pattern in the chondrite-normalized diagram (Fig. 9e). It further shows negative anomalies of Ba, Nb, Sr and Ti in the primitive mantle-normalized trace element diagram (Fig. 9f).

4.2.3. CTGB

The 895.6 Ma old granitic gneiss (sample DK28) is a granodiorite (Fig. 8a) ($Fe^*=0.81$, $\delta=1.43$ and A/CNK = 1.12) displaying a ferro-magnesian, strong peraluminous and calc-alkaline character. The sample has a moderate LREE-enrichment and flat HREE-pattern in the chondrite-normalized diagram with a slight negative Eu anomaly (Eu/Eu* of 0.64) (Fig. 9g). $(La/Yb)_N$ and $(Gd/Yb)_N$ are 7.02 and 1.40. It further shows relative depletions of Ba, Sr, Nb, Ta and Ti in the primitive mantle-normalized trace element diagram (Fig. 9h). The gneiss has a high initial $^{87}Sr/^{86}Sr$ ratio of 0.7170, a low $\varepsilon Nd_{(882Ma)}$ value of −14.1 and an Nd model age (T_{DM}) of 2.65 Ga (Chen et al., 1999a).

The granitoids with ages between 437.4 and 320.8 Ma plot in the gabbroic diorite, diorite, monzodiorite, monzonite, quartz monzonite, granodiorite and granite fields (Fig. 8a). Their δ value varies from 1.6 to 4.36, A/CNK from 0.66 to 1.07 and Fe* from 0.61 to 0.80, indicating a magnesian, metaluminous to weakly peraluminous, calc-alkaline to high-potassic composition. The chondrite-normalized rare earth element patterns for all samples are characterized by a moderate to strong LREE-enrichment, flat HREEs and a negative Eu anomaly (Fig. 9i and k). $(La/Yb)_N$ displays a large range from 2.29 to 18.57 and, accordingly $(Gd/Yb)_N$ from 1.06 to 2.40 and a Eu/Eu* anomaly from 0.64 to 0.95 (except sample QK5). All samples show negative anomalies for Ba, Sr, Nb, Ta and Ti in the primitive mantle-normalized trace elements (Fig. 9j and l). $(^{87}Sr/^{86}Sr)_i$ isotope ratios range from 0.7047 to 0.7163, εNd(t) from −6.5 to 2.03 and the samples have Nd model ages (T_{DM}) from 974 to 1749 Ma (Table S4; Fig. 10).

The 247.2 Ma old biotite–hornblende granodiorite (sample XT18) is magnesian, calc-alkaline and metaluminous ($Fe^*=0.73$, $\delta=1.83$ and A/CNK = 0.93). The REE pattern is characterized by a slight LREE-enrichment, flat HREEs and slight negative Eu anomaly with $(La/Yb)_N=6.9$, $(Gd/Yb)_N=1.91$ and $Eu/Eu^*=0.64$ (Fig. 9m). The trace elements exhibit negative anomalies for Sr, Nb, Ta and Ti (Fig. 9n). Furthermore, the quartz syenite with a SHRIMP U–Pb age of 275 Main the Kekesu river has a Nd model age (T_{DM}) of 1545 Ma, a high $(^{87}Sr/^{86}Sr)_i$ ratio and an $\varepsilon Nd_{(276\ Ma)}$ value of 0.7081 and −4.68, respectively (Sample KKS1; Table S4).

4.2.4. STGB

A hornblende biotite granite intrusion from the Heiyingshan area which revealed a SHRIMP zircon U–Pb age of 285 ± 4 Ma (see Fig. 2 of Long et al., 2008) has a Nd model age (T_{DM}) of 1013 Ma, a low $(^{87}Sr/^{86}Sr)_i$ ratio and an $\varepsilon Nd_{(285\ Ma)}$ value of 0.7032 and −4.35, respectively (Sample HYS73; Table S4).

5. Discussion

5.1. Continental growth in the Western Tianshan Orogen

5.1.1. The involvement of Precambrian basements

Granitoid rocks in the Western Tianshan Orogen are thought to have recorded the continental growth in this region. A systematic study of the strontium and neodymium isotope values of granitoid rocks exposed in the orogenic belt will help in understanding a potential mantle contribution to continental growth during the genesis of these rocks (e.g., Chen and Arakawa, 2005; Han et al., 1997; Samson and Patchett,

1991; Wang et al., 2009a; Whalen et al., 1996). Here, we discuss the continental growth of the Western Tianshan Orogen based on the geochronological, geochemical and Sr and Nd isotope data obtained in this study (Table 1) in conjunction with previously published data for 92 granitoids and some basaltic rocks in the area (Table S4).

The granitoids of the Western Tianshan Orogen have a much wider variation of Sr and Nd isotope ratios than those exposed in Western Junggar, Eastern Junggar, Alataw and Altay terranes (Fig. 10). $^{87}Sr/^{86}Sr$ ratios and $\varepsilon_{Nd}(t)$ values of Precambrian granitoids show relatively enriched isotope compositions; the 798 Ma granitic gneiss of the NYGB has $(^{87}Sr/^{86}Sr)_i$ isotope ratios between 0.7196 and 0.7207, ε_{Nd} (798 Ma) values from −4.4 to −6.4 and Nd model ages of 1.93 to 2.01 Ga (Chen et al., 1999b). The 882 Ma to 896 Ma granitic gneiss of the CTGB has a $(^{87}Sr/^{86}Sr)_i$ isotope ratio of 0.7170, an ε_{Nd}(882 Ma) of −14.1 and a Nd model age of 2.65 Ga (Chen et al., 1999a) and the 707 Ma granitic gneiss of the STGB has $(^{87}Sr/^{86}Sr)_i$ isotope ratios of 0.7076 to 0.7096, ε_{Nd}(707 Ma) values from −4.1 to −7.1 and Nd model ages of 1.7 to 1.96 Ga (Chen et al., 2000b). These data suggest that the Western Tianshan Orogen has an early-mid Proterozoic basement and that the recycling of old continental crust was involved during the syn-/post-orogenesis.

Moreover, Archean granitic gneisses have a SHRIMP zircon U–Pb age of 2791 ± 24 Ma and Paleoproterozoic granitic gneisses have ages of 2187 and 1789 Ma and are exposed in southern Kazakhstan (Kröner et al., 2007). Granulite-facies gneisses from the NYGB have a SIMS zircon U–Pb age of 1609 ± 40 Ma (Li et al., 2009), granulite

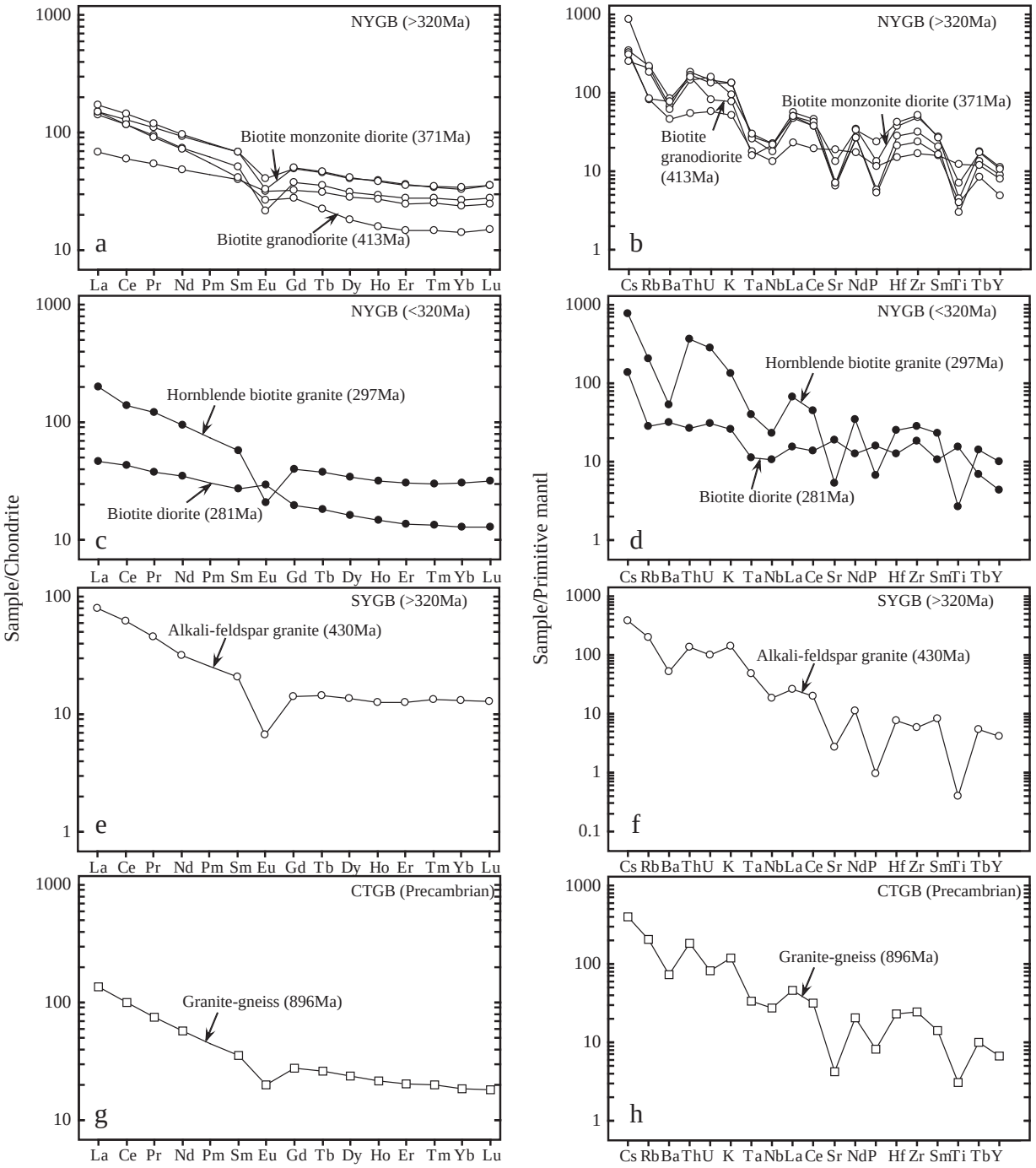

Fig. 9. Rare earth element pattern and trace element diagram of the granitoids (chondrite-normalized REE values are from Sun and McDonough (1989) and the primitive mantle normalized values are from Wood et al. (1979)). NYGB: The North Yili Block Granite Belt, SYGB: The South Yili Block Granite Belt, CTGB: The Central Tianshan Granite Belt.

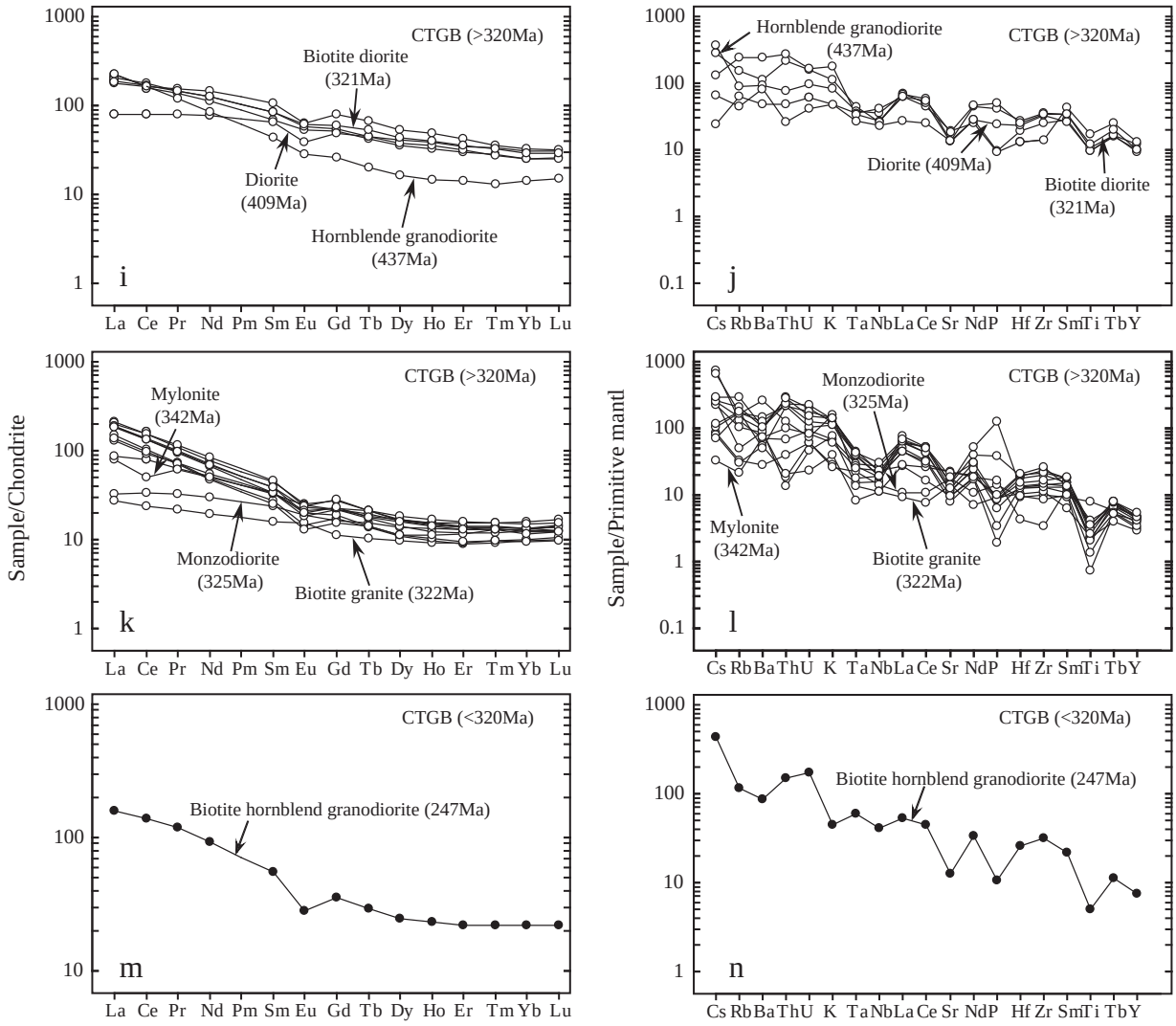

Fig. 9 (*continued*).

xenoliths from the Cretaceous Tuoyun basalts have LA-ICP-MS zircon U–Pb ages of 690 to 770 Ma and Hf model ages of 1.3–1.7 Ga (Zheng et al., 2006a, 2006b) and Tianshan basement rocks have Nd model ages of 1.7–2.2 Ga (Hu et al., 2000). These all indicate that substantial reworking of old crust during this period along the southwestern margin of the CAOB (Western Tianshan) may be more pronounced than in other parts of the CAOB, e.g., in the Western Junggar, Eastern Junggar, Alataw and Altay terranes (see Fig. 11).

5.1.2. Continental growth by accretion of arc complexes

Two current models have been established to explain the mechanism of the Phanerozoic continental growth in the CAOB: a) the 'syn-subduction continental growth by accretion of arc complexes related to oceanic subduction' (e.g., Sengör et al., 1993; Xiao et al., 2009a, 2009b) and b) the 'syn-subduction lateral continental growth by accretion of arc complexes as well as post-collisional vertical continental growth by accretion of mantle-derived material' (e.g., Han et al., 1997; Wang et al., 2009a). However, the exact timing of the final closure of the oceanic basins and amalgamation of the various terranes are essential for unraveling the mechanisms responsible for the Phanerozoic continental growth.

The Western Tianshan Orogen is characterized by the North Tianshan, Nikolaev Line-North Nalati and South Central Tianshan suture zones, which are representing the Junggar, Terskey and South Tianshan Oceans from north to south, respectively (present day geographic coordinate; Allen et al., 1992; Gao et al., 2009; Qian et al., 2009; Fig. 12a, b and c). The SHRIMP zircon U–Pb age of 316 ± 3 Ma for the undeformed Sikeshu ('stitching') pluton which crosscuts the suture zone indicates that the closure of the Junggar Ocean and the collision between the Yili block and Junggar terrane may have occurred between 325 and 316 Ma (Han et al., 2010a). The Terskey Ocean has been constrained to exist from the end of the Riphean (latest Neo-Proterozoic) until middle Early Ordovician (Lomize et al., 1997; Mikolaichuk et al., 1997). The collision between the Yili block and the Central Tianshan Arc terrane occurred at the end of Early Ordovician as a result of the closure of the Terskey Ocean (Qian et al., 2009). Following this collision, the Yili block and the Central Tianshan Arc terrane amalgamated as the new Yili block, the margin of which was superimposed by an active margin of the South Tianshan Ocean (or called Turkestan; Glorie et al., 2010; Seltmann et al., 2011). However, the Central Tianshan Arc terrane is thought to have been separated from the Tarim block by back-arc extension as a result of the subduction of the Terskey Ocean (Gao et al., 2009). The closure of the South Tianshan Ocean and the collision between the Yili and Tarim blocks happened at ca. 320 Ma according to the U–Pb ages of 319.5 ± 2.9 Ma and 318.7 ± 3.3 Ma obtained from eclogite-facies zircon rims from eclogites in the Chinese Tianshan (Su et al., 2010), a U–Pb age of 318 ± 7 Ma for rutile grains in eclogites (Li et al., 2011) and a Sm–Nd mineral and whole rock isochron age of 319 ± 4 Ma for an eclogite from the Kyrgyz Tianshan (Hegner et al., 2010).

Additionally, a U–Pb age of 284.8 ± 2.0 Ma obtained for zircon from a leucogranite dike crosscutting the high pressure–low temperature metamorphic belt further confirms a pre-Permian age for the collision between the Yili and Tarim blocks (Gao et al., 2011). Therefore, the closure of the Junggar and South Tianshan Oceans and the amalgamation of the Junggar terrane, and the Tarim and Yili-(Central Tianshan) blocks were completed by the beginning of the Late Carboniferous (Fig. 12d).

Thus, we propose that the genesis of granitoid rocks with an age older than 320 Ma in this study may be related to the subduction of paleo-oceans (Fig. 12b and c) because there is no evidence for post-collisional granitic intrusions related to the closure of the Terskey Ocean in the Chinese part.

This is supported by their geochemical characteristics with Nb–Ta troughs in the primitive mantle-normalized trace element diagrams (Fig. 9a, e, i and k) and the LREE-enrichment and flat HREEs in the chondrite normalized diagrams (Fig. 9b, f, g and k). Granitoids with an age younger than 320 Ma and less pronounced Nb–Ta anomalies (Fig. 9c and m) may have formed after the amalgamation of the Junggar terrane, and the Tarim and Yili-(Central Tianshan) blocks (Fig. 12d and e).

The Paleozoic granitoids (>320 Ma) display a more enriched Nd isotope composition when compared with those of the Western Junggar, Eastern Junggar, Alataw and Altay terranes (Figs. 10 and 11), also indicating that they are derived from a mixed source of the early-middle Proterozoic crust and a less enriched mantle in the Phanerozoic. The continental growth may thus be related to the subduction and accretion of the Terskey, the Junggar and the South Tianshan Oceans during the Paleozoic (>320 Ma; Fig. 12). The statistics of the zircon U–Pb ages obtained for the granitoids (Fig. 13a, b, c and d) support that granitic magmatism has made a great contribution to the continental growth.

A discussion of the continental growth of an orogen should also include an estimation of the proportion of crustal and mantle contributions to the evolution of granitic rocks (e.g., Mao et al., 2007; Wang et al., 2009a). The Neodymium Crustal Index (NCI) proposed by DePaolo (1985), DePaolo et al. (1992) and Perry et al. (1993) was used here ($NCI = [\varepsilon_{Nd}(rock) - \varepsilon_{Nd}(M)]/[\varepsilon_{Nd}(C) - \varepsilon_{Nd}(M)]$; where M and C refer to mantle and crust respectively). In the present study, a depleted mantle component is assumed to have an ε_{Nd}(425 Ma) value of +10, inferred from the neodymium isotopic value of the ophiolitic basalts in the Tianshan orogen (Long et al., 2006). An ε_{Nd} (425 Ma) of −14 is assigned for the crustal component according to the neodymium isotopic value of the granitic gneiss in the Tianshan orogen (Table S4) (Chen et al., 2000b). Calculation is undertaken using the $\varepsilon_{Nd}(t)$ values of granitoids with an age older than 320 Ma from the NYGB, the SYGB and the CTGB (Table S4). Although the NCI and the proportion of mantle component (PMC) values of individual plutons vary widely (Table S4, Fig. 14a, b, c, d and e), the average NCI value is 0.47, 0.55 and 0.36 indicating a PMC contribution of up to 53%, 45% and 64% for the granitoids (>320 Ma) from the NYGB, the SYGB and the CTGB, respectively. The mantle component used here is juvenile crust, which may have formed during the Paleozoic subduction of the Terskey, the Junggar and the South Tianshan Oceans. The PMC estimation suggests that almost half of the material necessary for the evolution of the granitoids was derived from the supra-subduction depleted mantle, resulting in the continental growth along the arc systems of the Western Tianshan Orogen in Paleozoic times (>320 Ma). However, several granitic intrusions with an average PMC value of 58% (Table S4) of the STGB have been excluded here due to uncertainties concerning their tectonic environment (Han et al., 2004; Zhu et al., 2008a, 2008b).

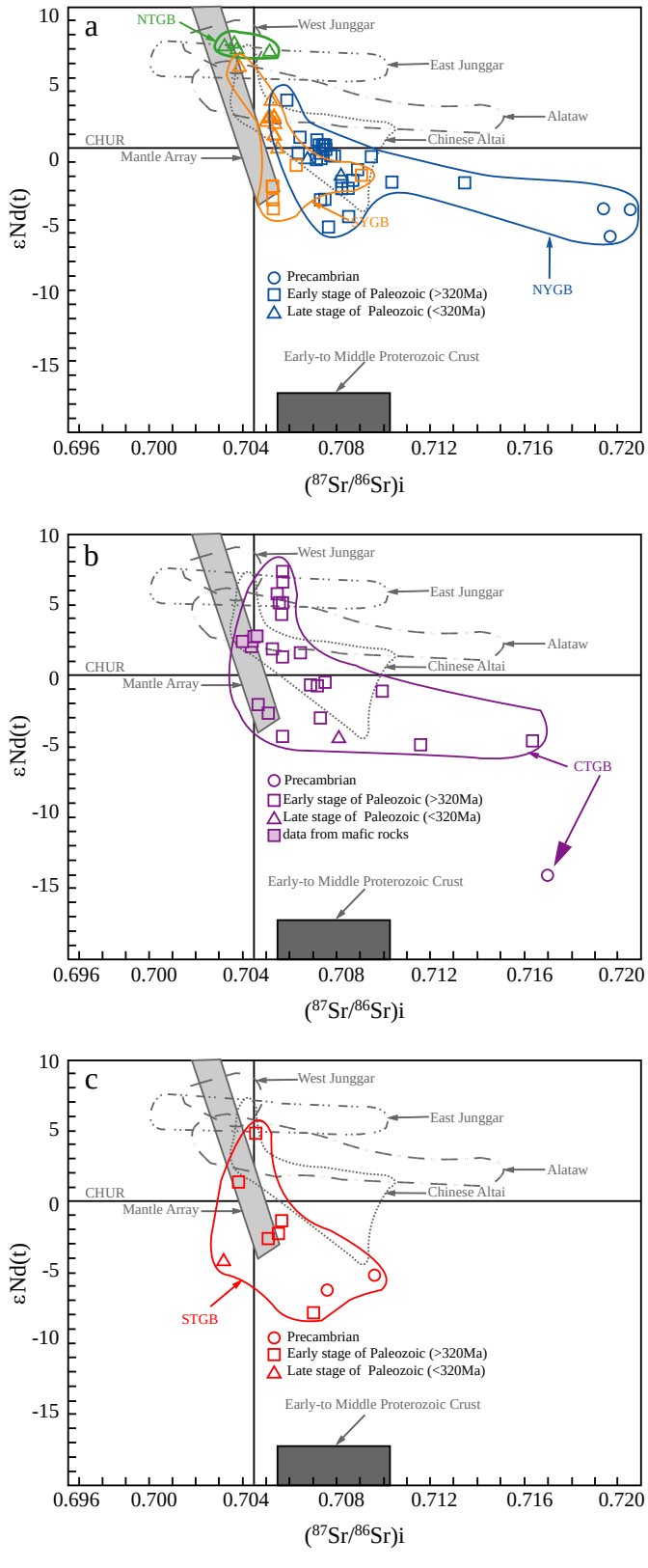

Fig. 10. Plot of initial Sr isotopic compositions $(^{87}Sr/^{86}Sr)_i$ versus εNd(t) values showing that the granitoids in the Western Tianshan Orogen have more enriched isotope compositions compared to the granitoids in the West Junggar, East Junggar, Alataw, and the Chinese Altay terranes. The Sr–Nd data for the Chinese Altay are from Wang et al. (2009a), for the West Junggar and Alataw from Chen and Arakawa (2005) and Chen and Jahn (2004), for the East Junggar from Chen and Jahn (2004), Han et al. (1997) and Tang et al. (2007). The data for the early to middle Proterozoic continental crust are after Hu et al. (2000). CHUR—chondrite uniform reservoir. NYGB: The North Yili Block Granite Belt, SYGB: The South Yili Block Granite Belt, CTGB: The Central Tianshan Granite Belt, STGB: South Tianshan Granite Belt.

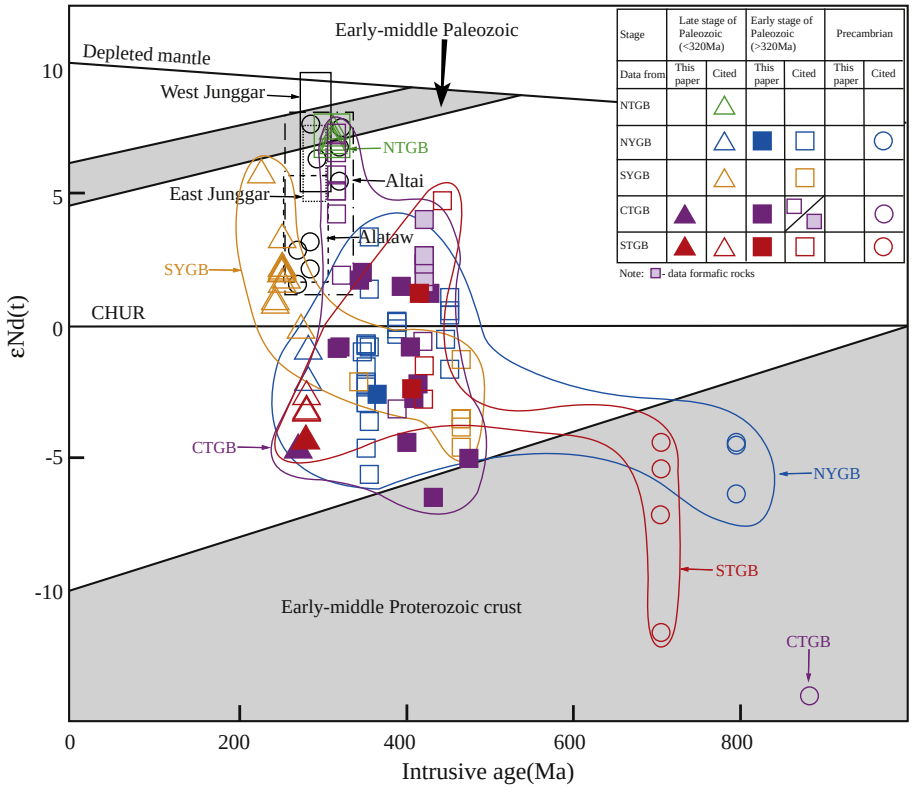

Fig. 11. Nd isotopic evolution of the early to middle Palaeozoic (Chen and Arakawa, 2005) and early to middle Proterozoic crust (Hu et al., 2000) and Nd isotope data of the granitoids in the Western Tianshan Orogen. Data source is in Table S4. NYGB: The North Yili Block Granite Belt, SYGB: The South Yili Block Granite Belt, CTGB: The Central Tianshan Granite Belt, STGB: South Tianshan Granite Belt.Nd isotopic evolution of the early to middle Palaeozoic (Chen and Arakawa, 2005) and early to middle Proterozoic crust (Hu et al., 2000) and Nd isotope data of the granitoids in the Western Tianshan Orogen. Data source is in Table S4. NYGB: The North Yili Block Granite Belt, SYGB: The South Yili Block Granite Belt, CTGB: The Central Tianshan Granite Belt, STGB: South Tianshan Granite Belt.

The Ordovician adakitic dacite of the SYGB with an $\varepsilon_{Nd}(467\ Ma) = +4.0$ was interpreted to have been generated by melting of subducted oceanic crusts of the Terskey Ocean beneath the Yili block (Wang et al., 2009b). However, the Ordovician adakitic diorite with $\varepsilon_{Nd}(470\ Ma)$ values from −4.5 to −1.3 from the same region likely formed by partial melting of garnet amphibolites from thickened lower crust in an island arc settings (Qian et al., 2009). The 366 Ma old Lamasu granodiorite porphyries of the NYGB evolved from a (subduction-derived) melt-metasomatized mantle wedge with subsequent assimilation of crustal basement rocks according to their negative $\varepsilon_{Nd}(t)$ value of −5.6 to −0.8 and positive $\varepsilon_{Hf}(t)$ value of +1.4 to +10.6 (Tang et al., 2010a). Therefore, both the addition of material from the melting of oceanic crust and underplating of arc basaltic lower crust above a subduction zone may have caused the continental growth in the arc system (Fig. 12b, c).

The 430 Ma Jingbulake mafic–ultramafic intrusion which is composed of pyroxene diorite, olivine gabbro and wehrlite has a positive $\varepsilon_{Nd}(t)$ (+1.6 to +4.0), and low $(^{87}Sr/^{86}Sr)_i$ isotope ratios (0.7039–0.7048), indicating that it originated from a less enriched mantle source (Yang and Zhou, 2009; Zhang et al., 2010b). Thus, the accretion of basaltic magmas derived from the metasomatic supra-subduction depleted mantle wedge to the crust has resulted in the addition of juvenile mantle components in the arc system (Fig. 12c). Contrastingly, those 437 to 321 Ma old arc-type granitoids of the SYGB and CTGB with relatively lower $\varepsilon_{Nd}(t)$ (−6.5 to +2.1), and higher $(^{87}Sr/^{86}Sr)_i$ isotope ratios (0.7052–0.7163) (Table S4) may have been derived from mixing of an enriched source and a mix of old continental basement and young accreted basaltic melts which were derived from the metasomatized upper mantle wedge (Fig. 12c).

This arc-forming process involves both recycling of Precambrian continental basement and the juvenile mantle component that may contribute to continental growth. Furthermore, the amphibolite (basaltic composition) of the NYGB, which has $(^{87}Sr/^{86}Sr)_i$ isotope ratios of 0.7060 to 0.7071 and $\varepsilon_{Nd}(455\ Ma)$ values from −1.7 to +1.1 (Hu et al., 2008) also indicates that mafic magma may have been added to the continent during the arc accretion related to subduction of the Junggar Ocean. However, the ~413–352 Ma old granitoids of the NYGB with $(^{87}Sr/^{86}Sr)_i$ isotope ratios of 0.70595 to 0.7135 and $\varepsilon_{Nd}(t)$ values from −5.63 to +3.4 (Table S4) further indicate that the granitic magma was generated during the interaction between the basaltic magmas derived from a juvenile mantle component of the metasomatic supra-subduction wedge and the arc continental basements (e.g., Zhang et al., 2010a), resulting in the continental growth by arc magma accretion.

5.1.3. Continental growth by the accretion of underplated material of mantle derivation during post-collisional period

Subsequent to the closure of the Junggar, Terskey and South Tianshan Oceans followed by the amalgamation of the Junggar terrane, and the Tarim and Yili-(Central Tianshan) blocks at ca. 320 Ma, the whole Western Tianshan Orogen was overprinted by post-collisional magmatism across the terrane boundaries (Fig. 12d). Granitic rocks with a zircon U–Pb age varying from 316 Ma to 247 Ma are exposed in the NTGB, the NYGB, the SYGB, the CTGB and the STGB (Fig. 13a, b, c and d).

Several possible mechanisms have previously been proposed for the evolution of post-orogenic magmas in an orogenic belt, including: (1) crustal overthickening (Douce et al., 1990; Karsli et al., 2010; Le Fort et al., 1987); (2) extensional collapse (Turner et al., 1999); (3) regional lithospheric delamination of the overriding plate (Chalot-Prat and Girbacea, 2000; Ilbeyli et al., 2004; Kay and Kay, 1993; Whalen et al., 1994); (4) linear delamination (slab break-off) (Davies and von Blanckenburg, 1995); and (5) lithospheric plate-scale strike-slip shearing (Konopelko et al., 2007; Seltmann et al., 2011).

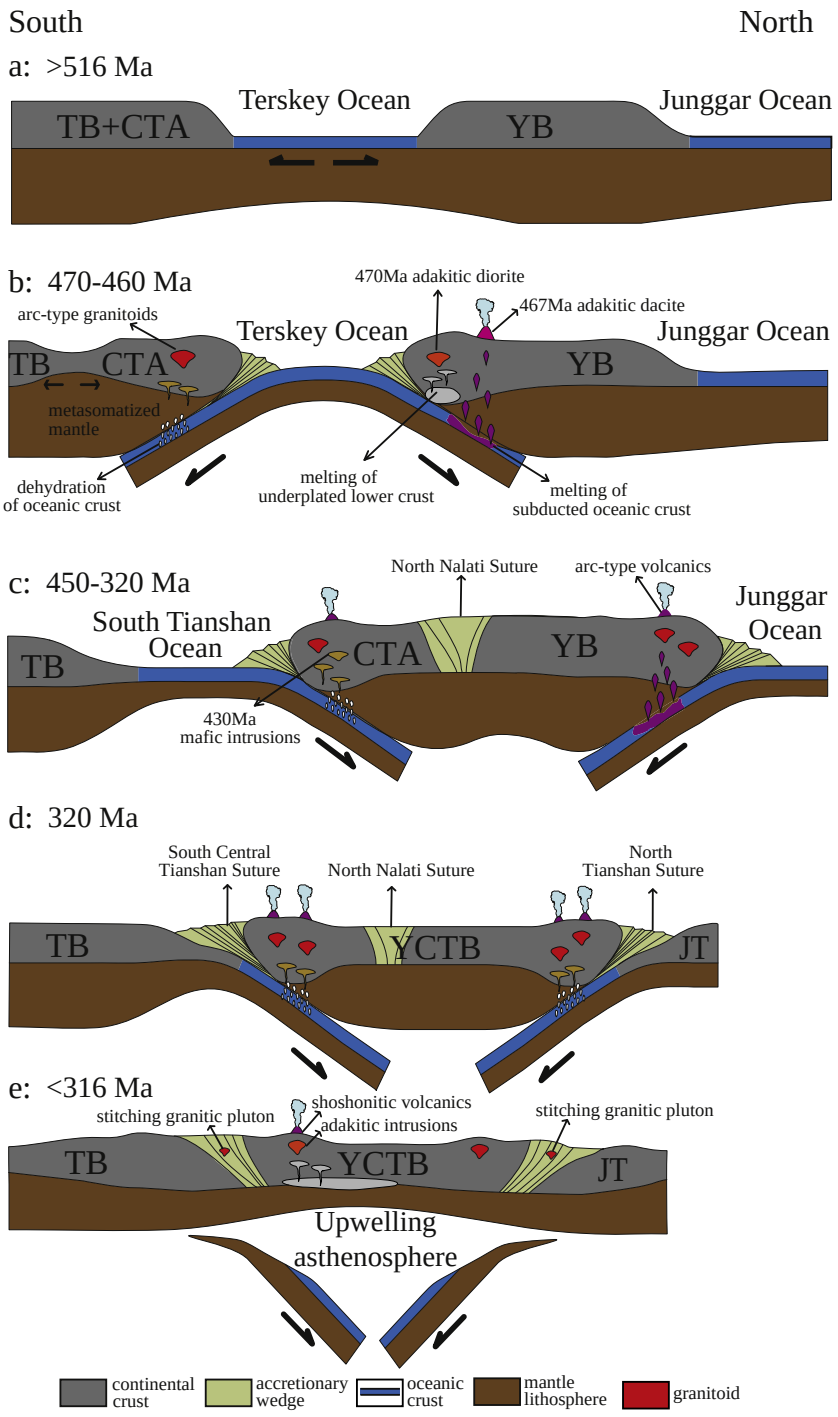

Fig. 12. Tectonic model showing the evolution and the continental growth mechanism of the Western Tianshan Orogen. TB: Tarim Block, CTA: Central Tianshan Arc, YB: Yili Block, JT: Junggar Terrane, YCTB: Yili-Central Tianshan Block.

The average NCI (Neodymium Crustal Index) values are 0.12, 0.43, 0.33, 0.61 and 0.56 for the post-collisional granitoids from the NTGB, the NYGB, the SYGB, the CTGB and the STGB, respectively (Table S4; Fig. 14) indicating that the average proportion of mantle component (PMC) values are up to 88%, 57%, 67%, 39% and 44%, respectively (Fig. 14f). The proportion of the mantle component of post-collisional granitoids is higher than that of the syn-subductional granitoids (Fig. 14f). A pronounced mantle component involved in the source of the post-collisional magmatism in the Western Tianshan Orogen argues against a 'crustal overthickening' model. This conclusion is further supported by the absence of associated Barrovian metamorphism and anatectic granitoid magmatism represented by S-type granites (Douce et al., 1990; Le Fort et al., 1987). Furthermore, the 'extensional collapse' model is unlikely to be responsible for the evolution of the post-collisional granitoids in the Western Tianshan Orogen, because no significant regional post-collisional extensional tectonics have been reported from this region (e.g., Lin et al., 2009). In addition, high temperature granulites and cordierite-bearing granites that are usually related to an extensional orogenic collapse (Turner et al., 1999) have not been observed. The delamination of lithosphere temporally results in rapid uplift, regional extension, massive crustal melting and mantle-derived magmatism (e.g., Kay and Kay, 1993; Turner et al., 1999). Although there is an obvious mantle component contribution to the source of the post-collisional magmas the lack of

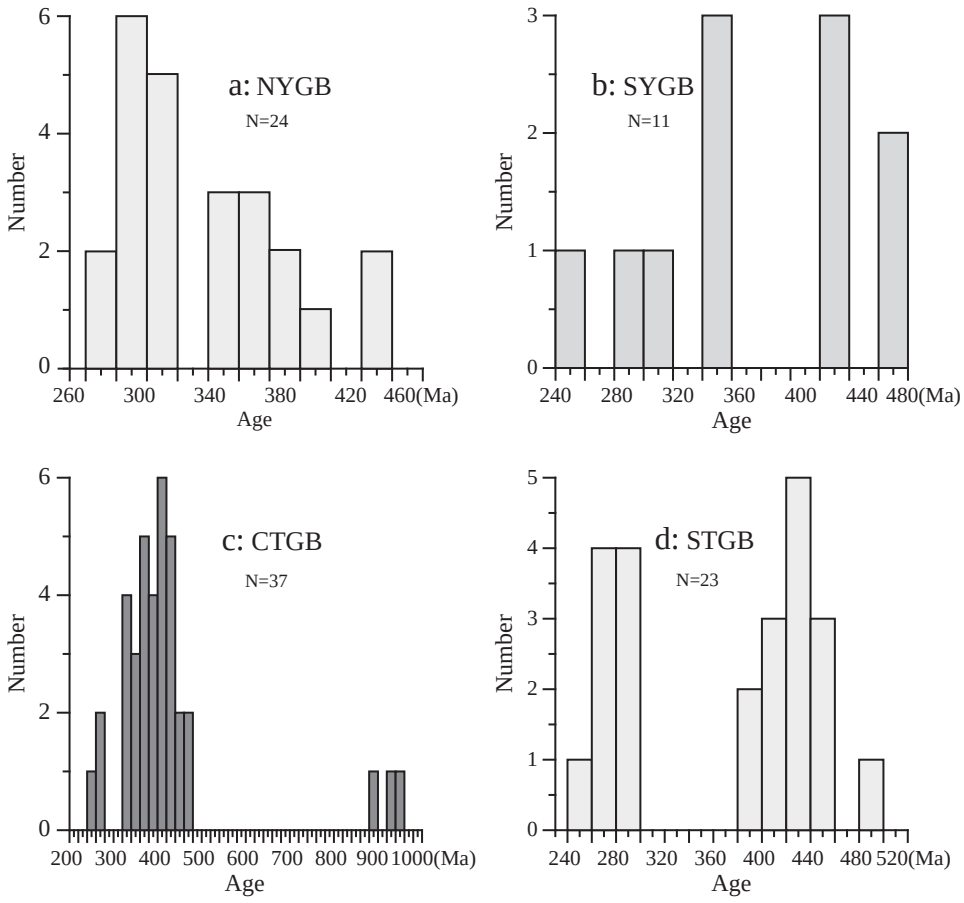

Fig. 13. Statistics of the zircon U–Pb ages obtained for the granitoids intruding into the Western Tianshan Orogen. Data are from Gao et al. (2009, 2011), Han et al. (2004 and 2010a), Hu et al. (2008), Li et al. (2010), Long et al. (2008), Shi et al. (2007), Tang et al. (2010a), Wang et al. (2006b), Xu et al. (2006), Yang et al. (2006a), Zhang et al. (2010a), Zhu et al. (2006a and 2006b, 2008a and 2008b), and this study.

regional extension tectonics, the generation of massive S-type granites through crustal melting and associated high-temperature metamorphism preclude a regional delamination in the Western Tianshan Orogen during the post-collisional period.

Linear delamination caused by slab breakoff (Davies and von Blanckenburg, 1995) may on the other hand be a reasonable mechanism to explain post-collisional magmatism in this region. The Sikeshu pluton of the NTGB has the lowest $(^{87}Sr/^{86}Sr)_i$ ranging from 0.70304 to 0.70421 and highest positive $\varepsilon_{Nd}(316\ Ma) = +6.8$ to $+7.3$ of all granitoids in the Western Tianshan Orogen (Fig. 10). It further has very young depleted-mantle Nd model ages (T_{DM}) of 462 to 516 Ma (Han et al., 2010a), indicating that the mantle-derived juvenile proportion is up to 88% for this granitic intrusion. These isotope characteristics are similar to those of the granitoids from the Western Junggar terrane, which were also interpreted as juvenile magmas (Figs. 10 and 11; Chen and Arakawa, 2005; Han et al., 2010a). Post-collisional basaltic underplating caused by slab breakoff and delamination of mantle lithosphere has potentially been established for the generation of these granitoids with depleted mantle-like Sr–Nd isotope characteristics (Han et al., 2010a). As a result of the breakoff of the previous Junggar Oceanic slab, the upwelling asthenosphere impinged on the lithosphere which had been metasomatized by fluids or melts derived by subduction dehydration. This process triggered the generation of basaltic melts, which were assimilated by the crustal basement, and this process eventually created several post-collisional granitoids (with a 57% mantle component proportion) of the NYGB.

Furthermore, the linear delamination (slab breakoff) can also explain the genesis of post-collisional granitoids (<320 Ma) of the SYGB, CTGB and STGB. The 260 Ma adakite of the SYGB has relatively lower $(^{87}Sr/^{86}Sr)_i$ isotope ratios of 0.7051 to 0.7054, higher ε_{Nd} (260 Ma) values of $+1.57$ to $+3.26$, and younger Nd model ages of 0.47 to 0.60 Ga (Zhao et al., 2008) than the subduction-related granitoids (>320 Ma; Table S4). These adakites were interpreted to have formed by partial melting of thickened lower crust under eclogite-facies conditions during the post-collisional tectonic process (Zhao et al., 2008). The breakoff of the subducted oceanic lithosphere represented by the South Tianshan Ocean and the delamination of the former metasomatized upper lithosphere may have supplied the required heat for the melting of thickened lower crust (Fig. 12e). The linear distribution of Permian shoshonitic volcanic rocks along the SYGB that are associated with the post-collisional adakites (Zhao et al., 2009) agree with a slab breakoff model (e.g., Karsli et al., 2010; Mao et al., 2007). However, the post-collisional granitoids of the CTGB and STGB display more enriched isotopic compositions and older Nd model ages than those of the SYGB, NYGB and NTGB (Figs. 10 and 11) implying the involvement of a crustal basement component. For example, the 276 Ma quartz syenite of the CTGB has a $(^{87}Sr/^{86}Sr)_i$ isotope ratio of 0.7081, an $\varepsilon_{Nd}(276\ Ma)$ of -4.68 and a Nd model age of 1.55 Ga. Thus, old continental material was involved during post-collisional magmatism of the CTGB and the STGB due to the relatively weaker delamination of the mantle lithosphere under the thickened continental crust. The average PMC estimated for the granitoids of the CTGB and STGB is 39% and 44% respectively (Table S4, Fig. 14f). These values are lower than those calculated for the granitoids of the SYGB, NYGB and NTGB (67%, 57% and 88% respectively; Table S4, Fig. 14f). However, there is a still significant contribution of mantle-derived components to the

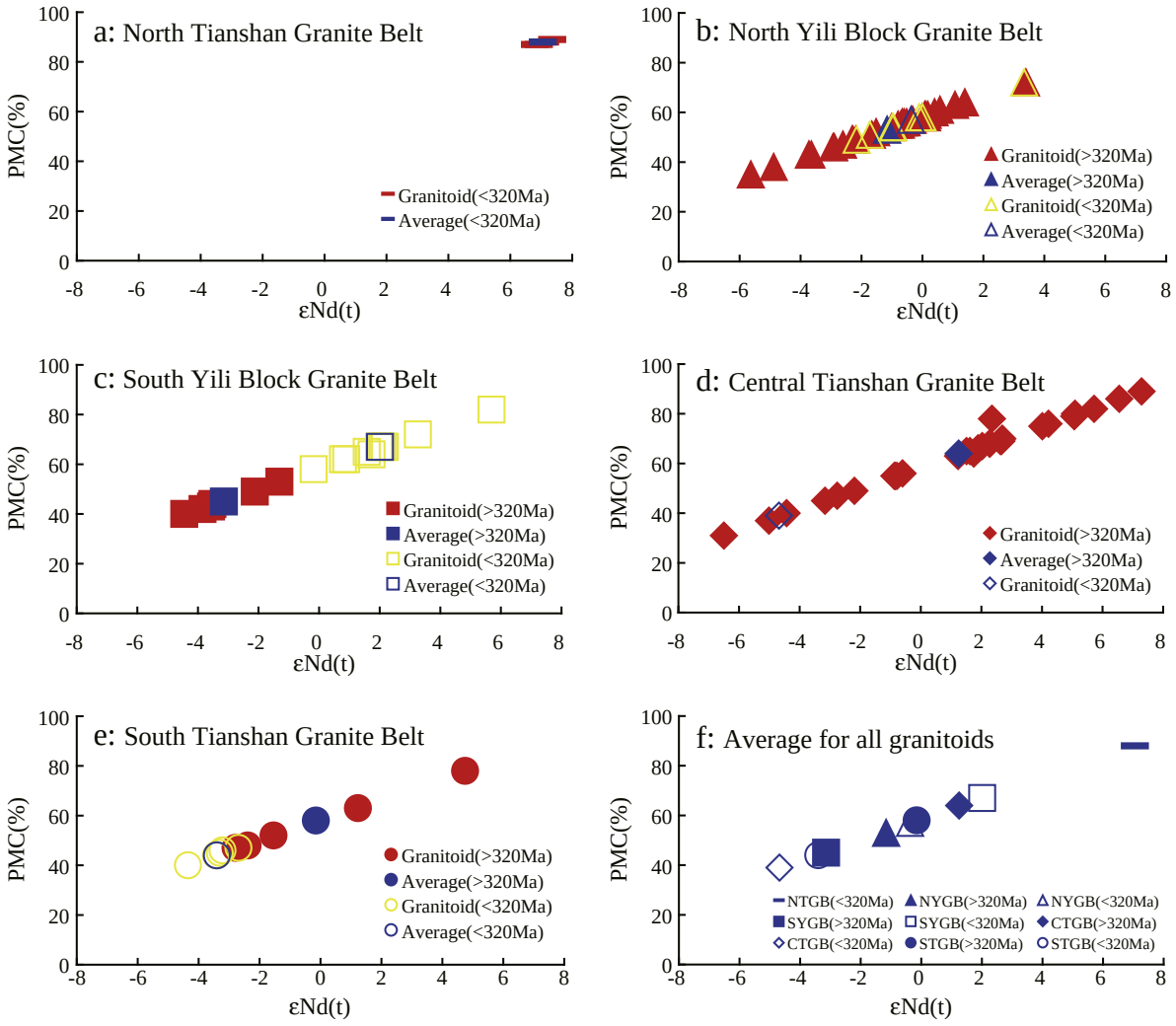

Fig. 14. Epsilon Nd versus Proportion of Mantle Components (PMC) diagram for granitoids in the Western Tianshan Orogen. NYGB: The North Yili Block Granite Belt, SYGB: The South Yili Block Granite Belt, CTGB: The Central Tianshan Granite Belt, STGB: South Tianshan Granite Belt.

magmatic source producing the granitoids of the CTGB and STGB. Therefore, continental growth occurred by accretion of underplated mantle materials during a tectonic process related to the post-collisional 'slab breakoff'.

5.2. Implications for the continental growth of the CAOB

Base on the studies presented here, we conclude that a substantial amount of reworking of early-middle Paleozoic crust has occurred in the Western Tianshan Orogen. During the oceanic subduction period (>320 Ma), growth of the continental crust is the result of the accretion of arc complexes and the juvenile mantle component. The juvenile components were derived from the addition of oceanic crustal melts (adakites) and the intrusion of basaltic melts from melting of a metasomatized depleted mantle (Fig. 12b, c). Both, adakitic melts and basaltic magmas may have mixed with continental basement material during ascend into the upper arc crust. Furthermore, post-collisional granitoid intrusions (<320 Ma) with their characteristically low Sr and higher Nd isotope signatures are sporadically and linearly exposed. The significant mantle component and linear distribution of post-collisional granitic plutons may favor a mechanism of delamination associated with slab breakoff. However, the post-collisional plutons occupy a relatively small area when compared with the >320 Ma granitoids. Therefore, the syn-subduction lateral growth of continental crust in arc settings (Fig. 12b, c) is thought to be the predominant mechanism responsible for the continental growth in the Western Tianshan Orogen. Contrastingly, the post-collisional vertical addition of juvenile mantle material (Fig. 12e) is thought to be of subordinate importance.

The average $\varepsilon_{Nd}(t)$ of granitoids in the Western Tianshan is around 0 (Table S4) indicating different proportions of old crustal material and juvenile mafic magmas. The average proportion of the mantle component (PMC) value is ca. 57% for all studied arc affinity granitoids and 63% for all post-collisional granitoids in the Western Tianshan Orogen, supporting that continental growth had been achieved by a 'two stage model' including both the 'syn-subductional accretion of arc complexes' and the 'post-collisional accretion of underplated material derived from the mantle' processes. This two stage model may also be a reasonable model for the continental growth of the western segment of the CAOB including northern Mongolia (Jahn et al., 2000), south Kazakhstan (Kröner et al., 2007, Kröner et al., 2008), central Altay (Wang et al., 2009a), Junggar (e.g., Chen and Arakawa, 2005; Han et al., 1997, 2010a; Wang et al., 2009a) and in the Western Tianshan.

However, Sengör et al. (1993) also hypothesized that nearly half of the CAOB may have been derived from the mantle by arc accretion. This one stage model of 'lateral continental growth by the accretion of arc complexes in active continental margins' has been suggested to be the only mechanism responsible for the continental growth in the CAOB (Xiao et al., 2009a, 2009b, 2010). This conclusion was based on

the final amalgamation of the southern active margin of Siberia with the passive margin of the Tarim block has lasted until mid-Triassic (Zhang et al., 2007; Xiao et al., 2009a). However, recent results (Gao et al., 2011; Su et al., 2010) demonstrate that the closure of all oceanic basins and the collision of the Tarim and Yili-Central Tianshan blocks were already completed by the end of the Early Carboniferous (ca. 320 Ma). Post-collisional granitoids, which resulted from slab break-off delamination, are linearly exposed in the Tianshan and predominantly occur along transcurrent faults (this study, Konopelko et al., 2007; Seltmann et al., 2011). Furthermore, the genesis of the Late Carboniferous to Permian gabbroic and granitic intrusions exposed in the Harlik Arc of the Eastern Chinese Tianshan Orogen has also been related to a slab break-off regime (Yuan et al., 2010).

The difference between the 'one-stage' and 'two-stage' models focuses on the widespread occurrence of late Carboniferous and Permian granitoids, including A-type granites and adakites and coeval Cu–Ni-sulfide-bearing, mafic–ultramafic complexes. Windley et al. (2007) and Xiao et al. (2009a and 2009b) interpreted the mafic–ultramafic intrusions as Alaskan-type mafic–ultramafic complexes which have formed in an accretionary wedge. A ridge subduction mechanism was employed to account for the increased heat necessary to cause partial melting of the crust generating the granitoids including adakites and high-Mg dacites and coeval mafic rocks (Geng et al., 2009; Han et al., 2010b; Tang et al., 2010b). In contrast, post-collisional basaltic underplating caused by slab breakoff or delamination of mantle lithosphere (Chen and Jahn, 2004; Han et al., 1997, 2010a; Jahn et al., 2000) or related to mantle plume rifting (Qin et al., 2011; Zhou et al., 2004) may be an alternative mechanism for the generation of these granitoids and coeval mafic–ultramafic rocks. Furthermore, Han et al. (2010a) precluded the possibility of a 'ridge subduction' mechanism (Geng et al., 2009; Windley et al., 2007) being responsible for the genesis of the late Carboniferous–Permian granitoids and coeval mafic–ultramafic magmatic complexes. The Yili block, the Junggar terranes and the Tarim block had coalesced already at the beginning of the late Carboniferous and thus no oceanic basin existed during the Permian anymore. Therefore, the late Carboniferous and Permian granitoids including A-type granites and adakites, and coeval Cu–Ni-sulfide-bearing, mafic–ultramafic complexes in North Xinjiang and contiguous regions of the CAOB were formed during the post-collisional orogenic period.

In summary, the two stage model, 'syn-subductional accretion of arc complexes' and 'post-collisional accretion of underplated mantle materials', may represent a reasonable model for the Phanerozoic continental growth of the western segment of the CAOB.

6. Conclusions

(1) The geochronological and Sr–Nd isotopic data presented here in conjunction with previously published data suggest a significant amount of recycling of older, early-middle Proterozoic crust in the Western Tianshan Orogen.
(2) The continental growth was accomplished via accretion of arc complexes during oceanic subduction (>320 Ma). A juvenile mantle component has been added by melting of oceanic crust and underplating to the island-arc lower crust and the intrusion of basaltic magmas derived from partial melting of a metasomatized depleted mantle wedge.
(3) The accretion of underplated mantle material may have been accomplished by a tectonic process related to 'slab breakoff' delamination during the post-collision period (<320 Ma).
(4) The two stage model, 'syn-subductional accretion of arc complexes' and 'post-collisional accretion of underplated mantle material', may represent a comprehensive model for the continental growth of the western segment of the CAOB in the Phanerozoic Eon.

Supplementary materials related to this article can be found online at doi:10.1016/j.lithos.2011.07.015.

Acknowledgments

This study was funded by the State Key Project for Basic Research of China (2007CB411304 and 2007CB411302), the National Natural Science Foundation of China (41025008, 40672153, 40721062, 40872057), China Geological Survey (1212010911070) and the DFG (KL 692/17-2,3). We are indebted to H. Li for conducting the XRF-analyses, X. D. Jin and H. Y. Li for their arrangement in the trace element analysis, B. Song and H. Tao for help during the SHRIMP dating, and X. M. Liu for help during the La-ICP-MS dating. We thank Mr. Y. G. Ma and Q. Mao for their help with the Cathodoluminescence (CL) images. ChB acknowledges the drillers of JOIDES Resolution for giving him a welcome break, as a result of a stuck drillbit, to work on the final changes in the preparation of the manuscript. The authors appreciate the constructive comments of Y. Chao and D. Konopelko on the manuscript.

References

Allen, M.B., Windley, B.F., Zhang, C., 1992. Palaeozoic collisional tectonics and magmatism of the Chinese Tien Shan, central Asia. Tectonophysics 220, 89–115.
Barbarin, B., 1999. A review of the relationships between granitoid types, their origins and their geodynamic environments. Lithos 46, 605–626.
Bazhenov, M.L., Collins, A.Q., Degtyarev, K.E., Levashova, N.M., Ikolaichuk, A.V., Pavlov, V.E., Van der Voo, R., 2003. Paleozoic northward drift of the North Tien Shan (Central Asia) as revealed by Ordovician and Carboniferous paleomagnetism. Tectonophysics 366, 113–141.
Carroll, A.R., Graham, S.A., Hendrix, M.S., Ying, D., Zhou, D., 1995. Late Paleozoic tectonic amalgamation of northwestern China: sedimentary record of the north Tarim, northwestern Turpan and southern Junggar basins. Geological Society of American Bulletin 107, 571–594.
Chalot-Prat, F., Girbacea, R., 2000. Partial delamination of continental mantle lithosphere, uplift-related crust–mantle decoupling, volcanism and basin formation: a new model for the Pliocene–Quaternary evolution of the southern East-Carpathians, Romania. Tectonophysics 327, 83–107.
Charvet, J., Shu, L.S., Laurent-Charvet, S., 2007. Paleozoic structural and geodynamic evolution of eastern Tianshan (NW China): welding of the Tarim amd Junggar plates. Episodes 30, 162–186.
Chen, B., Arakawa, Y., 2005. Elemental and Nd–Sr isotopic geochemistry of granitoids from the West Junggar foldbelt (NW China) with implications for Phanerozoic continental growth. Geochimica et Cosmochimica Acta 69, 1307–1320.
Chen, B., Jahn, B.M., 2004. Genesis of post-collisional granitoids and basement nature of the Junggar terrane, NW China: Nd–Sr isotope and trace element evidence. Journal of Asian Earth Sciences 23, 691–703.
Chen, Y.B., Hu, A.Q., Zhang, Q.F., 1999a. Zircon U–Pb age of granitic gneiss on Du–Ku highway in Western Tianshan of China and its geological implications. Chinese Science Bulletin 45, 649–653.
Chen, Y.B., Hu, A.Q., Zhang, G.X., 1999b. Zircon U–Pb age and Nd–Sr isotopic composition of granitic gneiss and its geological implications from Precambrian tectonic window of Western Tianshan, NW China. Geochemica 28, 515–520.
Chen, J.F., Zhou, T.X., Xie, Z., Zhang, X., Guo, X.S., 2000a. Formation of positive εNd(T) granitoids from the Alataw Mountains, Xinjiang, China, by mixing and fractional crystallization: implication for Phanerozoic crustal growth. Tectonophysics 328, 53–67.
Chen, Y.B., Hu, A.Q., Zhang, G.X., 2000b. Precambrian basement age and characteristics of SouthWestern Tianshan: Zircon U–Pb geochronology and Nd–Sr isotopic compositions. Acta Petrologica Sinica 16, 91–98 (in Chinese with English abstract).
Coleman, R.G., 1989. Continental growth of northwest China. Tectonics 8, 621–635.
Davies, J.H., von Blanckenburg, F., 1995. Slab breakoff: a model of lithosphere detachment and its test in the magmatism and deformation of collisional orogens. Earth and Planetary Science Letters 129, 85–102.
DePaolo, D.J., 1985. Isotope studies of processes in mafic magma chambers: I. Kiglapait Intrusion, Labrador. Journal of Petrology 26, 925–951.
DePaolo, D.J., Perry, F.V., Baldridge, W.S., 1992. Crustal versus mantle sources of granitic magmas: a two-parameter model based on Nd isotopic studies. Royal Society of Edinburgh Transactions: Earth Sciences 83, 439–446.
Douce, A.E.P., Humphreys, E.D., Johnston, A.D., 1990. Anatexis and metamorphism in tectonically thickened continental crust exemplified by the Sevier hinterland, western North America. Earth and Planetary Science Letters 97, 290–315.
Frost, B.R., Barnes, C.G., Collins, W.J., 2001. A geochemical classification for granitic rocks. Journal of Petrology 42, 2033–2048.
Gao, J., Klemd, R., 2003. Formation of HP-LT rocks and their tectonic implications in the Western Tianshan Orogen, NW China: geochemical and age constraints. Lithos 66, 1–22.
Gao, J., He, G.Q., Li, M.S., Tang, Y.Q., Xiao, X.C., Zhou, M., Wang, J., 1995. The mineralogy, petrology, metamorphic PTDt trajectory and exhumation mechanism of blueschists, south Tianshan, northwestern China. Tectonophysics 250, 151–168.

Gao, J., Li, M.S., Xiao, X.C., Tang, Y.Q., He, G.Q., 1998. Paleozoic tectonic evolution of the Tianshan orogen, northwestern China. Tectonophysics 287, 213–231.
Gao, J., Klemd, R., Zhang, L.F., Wang, Z.X., Xiao, X.C., 1999. P–T path of high pressure–low temperature rocks and tectonic implications in the Western Tianshan Mountains (NW China). Journal of Metamorphic Geology 17, 621–636.
Gao, J., Long, L.L., Klemd, R., Qian, Q., Liu, D.Y., Xiong, X.M., Su, W., Liu, W., Wang, Y.T., Yang, F.Q., 2009. Tectonic evolution of the South Tianshan orogen and adjacent regions, NW China: geochemical and age constraints of granitoid rocks. International Journal of Earth Sciences 98, 1221–1238.
Gao, J., Klemd, R., Qian, Q., Zhang, X., Li, J.L., 2011. The collision between the Yili and Tarim blocks of the Southwestern Altaids: geochemical and age constraints of a leucogranite dike crosscutting the HP–LT metamorphic belt in the Chinese Tianshan Orogen. Tectonophysics 499, 118–131.
Geng, H.Y., Sun, M., Yuan, C., Xiao, W.J., Xian, W.S., Zhao, G.C., Zhang, L.F., Wong, K., Wu, F.Y., 2009. Geochemical, Sr–Nd and zircon U–Pb–Hf isotopic studies of Late Carboniferous magmatism in the West Junggar, Xinjiang: implications for ridge subduction? Chemical Geology 266, 364–389.
Glorie, S., Grave, J.D., Buslov, M.M., Elburg, M.A., Stockli, D.F., Gerdes, A., Van den Haute, P., 2010. Multi-method chronometric constraints on the evolution of the Northern Kyrgyz Tien Shan granitoids (Central Asian Orogenic Belt): from emplacement to exhumation. Journal of Asian Earth Sciences 38, 131–146.
Han, B.F., Wang, S.G., Jahn, B.M., Hong, D.W., Kagami, H., Sun, Y.L., 1997. Depleted-mantle magma source for the Ulungur River A-type granites from north Xinjiang, China: geochemistry and Nd–Sr isotopic evidence, and implication for Phanerozoic crustal growth. Chemical Geology 138, 135–159.
Han, B.F., He, G.Q., Wu, T.R., Li, H.M., 2004. Zircon U–Pb dating and geochemical features of early Paleozoic granites from Tianshan, Xinjiang: implications for tectonic evolution. Xinjiang Geology 22, 4–11 (in Chinese with English abstract).
Han, B.F., Ji, J.Q., Song, B., Chen, L.H., Zhang, L., 2006. Late Paleozoic vertical growth of continental crust around the Junggar Basin, Xinjiang, China (part I): timing of post-collisional plutonism. Acta Petrologica Sinica 22, 1077–1086 (in Chinese with English abstract).
Han, B.F., Guo, Z.J., Zhang, Z.C., Zhang, L., Chen, J.F., Song, B., 2010a. Age, geochemistry, and tectonic implications of a late Paleozoic stitching pluton in the North Tian Shan suture zone, Western China. Geological Society of American Bulletin 122, 627–640.
Han, C.M., Xiao, W.J., Zhao, G.C., Ao, S.J., Zhang, J., Qu, W.J., Du, A.D., 2010b. In-situ U–Pb, Hf and Re–Os isotopic analyses of the Xiangshan Ni–Cu–Co deposit in Eastern Tianshan (Xinjiang), Central Asian Orogenic Belt: constraints on the timing and genesis of the mineralization. Lithos 120, 547–562.
Hegner, E., Klemd, R., Kröner, A., Corsini, M., Alexeiev, D.V., Iaccheri, L.M., Zack, T., Dulski, P., Xia, X., Windley, B.F., 2010. Mineralogy ages and P–T conditions of late Paleozoic high-pressure eclogite and provenance of mélange sediments in the South Tianshan Orogen of Kyrgyzstan. American Journal of Science 310, 916–950.
Heinhorst, J., Lehmann, B., Ermolov, P., Serykh, V., Zhurutin, S., 2000. Paleozoic crustal growth and metallogeny of Central Asia: evidence from magmatic-hydrothermal ore systems of Central Kazakhstan. Tectonophysics 328, 69–87.
Hopson, C., Wen, J., Tilton, G., Tang, Y.Q., Zhu, B.Q., Zhao, M., 1989. Paleozoic plutonism in East Junggar, Bogdashan, and eastern Tianshan, NW China. EOS, Trans. American Geophysical Union 70, 1403–1404.
Hu, A.Q., Jahn, B.M., Zhang, G.X., Zhang, Q.F., 2000. Crustal evolution and Phanerozoic crustal growth in northern Xinjiang: Nd–Sr isotopic evidence. Part I: Isotopic characterisation of basement rocks. Tectonophysics 328, 15–51.
Hu, A.Q., Wei, G.J., Zhang, J.B., Deng, W.F., Chen, L.L., 2008. SHRIMP U–Pb ages for zircons of the amphibolites and tectonic evolution significance from the Wenquan domain in the West Tianshan Mountains, Xinjiang, China. Acta Petrologica Sinica 24, 2731–2740.
Ilbeyli, N., Pearce, J.A., Thirlwall, M.F., Mitchell, J.G., 2004. Petrogenesis of collision-related plutonics in Central Anatolia, Turkey. Lithos 72, 163–182.
Jahn, B.M., 2004. Phanerozoic continental growth in Central Asia. Journal of Asian Earth Sciences 23, 599–603.
Jahn, B.M., Wu, F.Y., Chen, B., 2000. Massive granitoid generation in Central Asia: Nd isotope evidence and implication for continental growth in the Phanerozoic. Episodes 23, 82–92.
Jahn, B.M., Capdevila, R., Liu, D.Y., Vernon, A., Badarch, G., 2004. Sources of Phanerozoic granitoids in the transect Bayanhongor–Ulaan Baatar, Mongolia: geochemical and Nd isotopic evidence, and implications for Phanerozoic crustal growth. Journal of Asian Earth Sciences 23, 629–653.
Karsli, O., Dokuz, A., Uysal, I., Aydin, F., Kandemir, R., Wijbrans, J., 2010. Generation of the Early Cenozoic adakitic volcanism by partial melting of mafic lower crust, Eastern Turkey: Implications for crustal thickening to delamination. Lithos 114, 109–120.
Kay, R.W., Kay, S.M., 1993. Delamination and delamination magmatism. Tectonophysics 219, 177–189.
Konopelko, D., Biske, G., Seltmann, R., Eklund, O., Belyatsky, B., 2007. Hercynian post-collisional A-type granites of the Kokshaal Range, Southern Tien Shan. Lithos 97, 140–160.
Konopelko, D., Biske, G., Seltmann, R., Kiseleva, M., Matukov, D., Sergeev, S., 2008. Deciphering Caledonian events: timing and geochemistry of the Caledonian magmatic arc in the Kyrgyz Tien Shan. Journal of Asian Earth Sciences 32, 131–141.
Kröner, A., Windley, B.F., Badarch, G., Tomurtogoo, O., Hegner, E., Jahn, B.M., Gruschka, S., Khain, E.V., Demoux, A., Wingate, M.T.D., 2007. Accretionary growth and crust formation in the Central Asian Orogenic Belt and comparison with the Arabian-Nubian shield. In: Hatcher, R.D., Carlson, M.P., McBride, J.H., Martínez Catalán, J.R. (Eds.), 4-D Framework of Continental Crust: Geological Society of American Memoir, 200, pp. 181–209.
Kröner, A., Hegner, E., Lehmann, B., Heinhorst, J., Wingate, M.T.D., Liu, D.Y., Ermelov, P., 2008. Palaeozoic arc magmatism in the Central Asian Orogenic Belt of Kazakhstan: SHRIMP zircon ages and whole-rock Nd isotopic systematic. Journal of Asian Earth Sciences 32, 118–130.
Le Fort, P., Cuney, M., Deniel, C., France-Lanord, C., Sheppard, S.M.F., Upreti, B.N., Vidal, P., 1987. Crustal generation of the Himalayan leucogranites. Tectonophysics 134, 39–57.
Li, H.Q., Wang, D.H., Wan, Y., Qu, W.J., Zhang, B., Luo, Y.F., Mei, Y.P., Zhou, Z.L., 2006. Isotopic geochronology study and its significance of the Lailisigao'er Mo deposit. Xinjiang. Acta Petrologica Sinica 22, 2437–2443 (in Chinese with English abstract).
Li, J.L., Su, W., Zhang, X., Liu, X., 2009. Zircon Cameca U–Pb dating and its significance for granulite-facies gneisses from the western Awulale Mountains, Western Tianshan. China. Geological Bulletin of China 28, 1852–1862 (in Chinese with English abstract).
Li, J.L., Qian, Q., Gao, J., Su, W., Zhang, X., Liu, X., Jiang, T., 2010. Geochemistry, zircon U–Pb ages and tectonic settings of the Dahalajunshan volcanics and granitic intrusions from the Adengtao area in the Southeast Zhaosu, western Tianshan Mountains. Acta Petrologica Sinica 26 (10), 2913–2924.
Li, Q.L., Lin, W., Su, W., Li, X.H., Shi, Y.H., Liu, Y., Tang, G.Q., 2011. SIMS U–Pb rutile age of low-temperature eclogites from southwestern Chinese Tianshan, NW China. Lithos 122, 76–86.
Lin, W., Faure, M., Shi, Y., Wang, Q., Li, Z., 2009. Palaeozoic tectonics of the south-western Chinese Tianshan: new insights from a structural study of the high-pressure/low-temperature metamorphic belt. International Journal of Earth Sciences 98, 1259–1274.
Liu, Y.M., Yang, W.H., Gai, J.Y., 1994. Study on isotopic age of Dahalajunshan formation in Tekesi forestry of Xinjiang. Geochimica 23, 99–104.
Liu, C.X., Xu, B.L., Zhou, T.R., 2004. Petrochemistry and tectonic significance of Hercynian alkaline rocks along the northern margin of the Tarim platform and its adjacent area. Xinjiang Geology 22 (1), 43–49 (in Chinese with English abstract).
Lomize, M.G., Demina, L.I., Zarshchicov, A.V., 1997. The Kyrgyz-Terskei paleoceanic basin in the Tien Shan. Geotectonics 31 (6), 463–482 (in Russian with English abstract).
Long, L.L., 2007. Paleozoic tectonic evolution and continental growth of the West Tianshan Orogen: evidence from granitoids and ophiolites. Ph. D. thesis, Chinese Academy of Sciences, Beijing, China (in Chinese with English abstract).
Long, L.L., Gao, J., Xiong, X.M., Qian, Q., 2006. The geochemical characteristics and the age of the Kule Lake ophiolite in the southern Tianshan. Acta Petrologica Sinica 22 (1), 65–73 (in Chinese with English abstract).
Long, L.L., Gao, J., Qian, Q., Xiong, X.M., Wang, J.B., Wang, Y.W., Wang, L.J., 2008. Geochemistry and SHRIMP Zircon U–Pb age of post-collisional granites in the Southwest Tianshan Orogenic Belt of China: examples from the Heiyingshan and Laohutai Plutons. Acta Geologica Sinina 82 (2), 415–424.
Maniar, P.D., Piccoli, P.M., 1989. Tectonic discrimination of granitoids. Geological Society of American Bulletin 101, 635–643.
Mao, X.X., Hou, Z.Q., Niu, Y.L., Dong, G.C., Qu, X.M., Zhao, Z.D., Yang, Z.M., 2007. Mantle contributions to crustal thickening during continental collision: evidence from Cenozoic igneous rocks in southern Tibet. Lithos 96, 225–242.
Middlemost, E.A.K., 1994. Naming materials in the magma/igneous rocks system. Earth Science Review 37, 215–224.
Mikolaichuk, A.V., Kurenkov, S.A., Degtyarev, K.E., Rubtsov, V.I., 1997. Main stages of geodynamic evolution of the North Tien Shan in the late Precambrian and early Paleozoic. Geotectonics 31, 16–34.
Peccerillo, R., Taylor, S.R., 1976. Geochemistry of Eocene calc-alkaline volcanic rocks from the Kastamonu area, northern Turkey. Contributions to Mineralogy and Petrology 58, 63–81.
Perry, F.V., DePaolo, D.J., Baldridge, W.S., 1993. Neodymium isotopic evidence for decreasing crustal contributions to Cenozoic ignimbrites of the western United States: implications for the thermal evolution of the Cordilleran crust. Geological Society of America Bulletin 105, 872–882.
Qian, Q., Gao, J., Klemd, R., He, G.Q., Xiong, X.M., Long, L.L., Liu, D.Y., Xu, R.H., 2009. Early Paleozoic tectonic evolution of the Chinese South Tianshan Orogen: constraints from SHRIMP zircon U–Pb geochronology and geochemistry of basaltic and dioritic rocks from Xiate, NW China. International Journal of Earth Sciences 98, 551–569.
Qin, K.Z., Su, B.X., Sakyi, P.A., Tang, D.M., Li, X.H., Sun, H., Xiao, Q.H., Liu, P.P., 2011. SIMS zircon U–Pb geochronology and Sr–Nd isotopes of Ni–Cu-bearing mafic–ultramafic intrusions in Eastern Tianshan and Beishan in correlation with flood basalts in Tarim basin (NW China): constraints on a ca. 280 Ma mantle plume. American Journal of Science 311. doi:10.2475/04.2011.00.
Rubatto, D., Gebauer, D., 2000. Use of cathodoluminescence for U–Pb zircon dating by ion microprobe: some examples from the Western Alps. In: Pagel, M., Barbi, V., Blanc, P., Ohnenstetter, D. (Eds.), Cathodoluminescence in Geosciences. Springer, Berlin Heidelberg New York, pp. 373–400.
Samson, S.D., Patchett, P.J., 1991. The Canadian Cordillera as a modern analogue of Proterozoic crustal growth. Australian Journal of Earth Sciences 38, 595–611.
Seltmann, R., Konopelko, D., Biske, G., Divaev, F., Sergeev, S., 2011. Hercynian post-collisional magmatism in the context of Paleozoic magmatic evolution of the Tien Shan orogenic belt. Journal of Asian Earth Sciences. doi:10.1016/j.jseaes.2010.08.016.
Sengör, A.M.C., Natal'in, B.A., Burtman, V.S., 1993. Evolution of the Altaid tectonic collage and Paleozoic crustal growth in Eurasia. Nature 364, 299–307.
Shi, Y.R., Liu, D.Y., Zhang, Q., Jian, P., Zhang, F.Q., Miao, L.C., 2007. SHRIMP zircon U–Pb dating of the Gangou granitoids, Central Tianshan Mountains, Northwest China and tectonic significances. Chinese Science Bulletin 52, 1507–1516.
Solomovich, L.I., 2007. Postcollisional magmatism in the South Tien Shan Variscan orogenic belt, Kyrgyztan: evidence for high-temperature and high-pressure collision. Journal of Asian Earth Sciences 30, 142–153.

Su, W., Gao, J., Klemd, R., Li, J.L., Zhang, X., Li, X.H., Chen, N.S., Zhang, L., 2010. U–Pb zircon geochronology of the Tianshan eclogites in NW China: implication for the collision between the Yili and Tarim blocks of the southwestern Altaids. European Journal of Mineralogy 22, 473–478.

Sun, S.S., McDonough, W.F., 1989. Chemical and isotopic systematics of ocean basalts: implications for mantle composition and processes. In: Saunders, A.D., Norry, M.J. (Eds.), Magmatism in Ocean Basin: Geological Society of London Special Publication, 42, pp. 313–345.

Sun, M., Yuan, C., Xiao, W.J., Long, X.P., Xia, X.P., Zhao, G.C., Lin, S.F., Wu, F.Y., Kröner, A., 2008. Zircon U–Pb and Hf isotopic study of gneissic rocks from the Chinese Altai: progressive accretionary history in the early to middle Palaeozoic. Chemical Geology 247, 352–383.

Tang, H.F., Qu, W.J., Su, Y.P., Hou, G.S., Du, A.D., Cong, F., 2007. Genetic connection of Sareshike tin deposit within the alkaline A-type granites of Sabei body in Xinjiang, constraint from isotopic ages. Acta Petrologica Sinica 23, 1989–1997.

Tang, G.J., Wang, Q., Wyman, D.A., Sun, M., Li, Z.X., Zhao, Z.H., Sun, W.D., Jia, X.H., Jiang, Z.Q., 2010a. Geochronology and geochemistry of Late Paleozoic magmatic rocks in the Lamasu–Dabate area, northwestern Tianshan (west China): evidence for a tectonic transition from arc to post-collisional setting. Lithos 119, 393–411.

Tang, G.J., Wang, Q., Wyman, D.A., Li, Z.X., Zhao, Z.H., Jia, X.H., Jiang, Z.Q., 2010b. Ridge subduction and crustal growth in the Central Asian Orogenic Belt: evidence from Late Carboniferous adakites and high-Mg diorites in the western Junggar region, northern Xinjiang (west China). Chemical Geology 277, 281–300.

Turner, S.P., Platt, J.P., George, R.M.M., Kelley, S.P., Pearson, D.G., Nowell, G.M., 1999. Magmatism associated with orogenic collapse of the Betic–Alboran Domain, SE Spain. Journal of Petrology 40, 1011–1036.

Wang, Z.X., Wu, J.Y., Liu, C.H., Lu, X.C., Zhang, J.G., 1990. Polycyclic Tectonic Evolution and Metallogeny of the Tianshan Mountains. Science Press, Beijing. (217 pp. in Chinese with English abstract).

Wang, B.Y., Lang, Z.J., Li, X.D., 1994. Study on the Geological Sections Across the Western Segment of Tianshan Mountains, China. Science Press, Beijing, pp. 1–202 (in Chinese).

Wang, T., Hong, D.W., Jahn, B.M., Tong, Y., Wang, Y.B., Han, B.F., Wang, X.X., 2006a. Timing, petrogenesis and setting of Paleozoic synorogenic intrusions from the Altai Mountains, northwest China: implications for the tectonic evolution of an accretionary orogen. Journal of Geology 114, 735–751.

Wang, B., Faure, M., Cluzel, D., Shu, L.S., Charvet, J., Meffre, S., 2006b. Late Paleozoic tectonic evolution of the northern West Tianshan, NW China. Geodinamica Acta 19, 237–247.

Wang, B., Shu, L.S., Cluzel, D., Faure, M., Charvet, J., 2007. Geochemical constraints on carboniferous volcanic rocks of Yili block (Xinjiang, NW China): implication for the tectonic evolution of Western Tianshan. Journal of Asian Earth Sciences 29, 148–159.

Wang, T., Jahn, B.M., Kovach, V.P., Tong, Y., Hong, D.W., Han, B.F., 2009a. Nd–Sr isotopic mapping of the Chinese Altai and implications for continental growth in the Central Asian orogenic belt. Lithos 110, 359–372.

Wang, Y.L., Qian, Q., Gao, J., Xiong, X.M., He, G.Q., Klemd, R., 2009b. Ordovician adakites from the northern part of the Nalati Mountains, Xinjiang (NW China). Changchun 2009, National Petrological and geodynamic conference (abstract): p.

Whalen, J.B., Jenner, G.A., Currie, K.L., Barr, S.M., Longstaffe, F.J., Hegner, E., 1994. Geochemical and isotopic characteristics of granitoids of the Avalon Zone, Southern Brunswick: possible evidence for repeated delamination events. Journal of Geology 102, 269–282.

Whalen, J.B., Jenner, G.A., Longstaff, F.J., Robert, F., Galiépy, C., 1996. Geochemical and isotopic (O, Nd, Pb and Sr) constraints on A-type granite petrogenesis based on the Topsails igneous suite, Newfoundland Appalachians. Journal of Petrology 37, 1463–1489.

Williams, I.S., 2001. Response of detrital zircon and monazite, and their U–Pb isotopic systems, to regional metamorphism and host-rock partial melting, Cooma Complex, southeastern Australia. Australian Journal of Earth Sciences 48, 557–580.

Windley, B.F., Alexeiev, D., Xiao, W.J., Kröner, A., Badarch, G., 2007. Tectonic models for accretion of the Central Asian orogenic belt. Journal of the Geological Society of London 164, 31–47.

Wood, D.A., Joron, J.L., Treuil, M., Norry, M., Tarney, J., 1979. Elemental and Sr isotope variations in basic lavas from Iceland and the surrounding ocean floor. Contributions to Mineralogy and Petrology 70, 3219–3339.

Xiao, X.C., Tang, Y.Q., Feng, Y.M., Zhu, B.Q., Li, J.Y., Zhao, M., 1992. Tectonic Evolution of Northern Xinjiang and Its Adjacent Regions. Geological Publishing House, Beijing. (169 pp. in Chinese with English abstract).

Xiao, W.J., Windley, B.F., Huang, B.C., Han, C.M., Yuan, C., Chen, H.L., Sun, M., Sun, S., Li, J.L., 2009a. End-Permian to mid-Triassic termination of the accretionary processes of the southern Central Asian Orogenic Belt: implications for the geodynamic evolution, Phanerozoic continental growth, and metallogeny of Central Asia. International Journal of Earth Sciences 98, 1189–1217.

Xiao, W.J., Windley, B.F., Yuan, C., Sun, M., Han, C.M., Lin, S.F., Chen, H.L., Yan, Q.R., Liu, D.Y., Qin, K.Z., Li, J.Y., Sun, S., 2009b. Paleozoic multiple subduction–accretion processes of the southern Altaids. American Journal of Science 309, 221–270.

Xiao, W.J., Huang, B.C., Han, C.M., Sun, S., Li, J.L., 2010. A review of the western part of the Altaids: a key to understanding the architecture of accretionary orogens. Gondwana Research 18, 253–273.

Xu, X.Y., Ma, Z.P., Xia, Z.C., Xia, L.Q., Li, X.M., Wang, L.S., 2006. TIMS U–Pb isotopic dating and geochemical characteristics of paleozoic granitic rocks from the middle-western section of Tianshan. Northwest Geology 39, 50–75 (in Chinese with English abstract).

Yang, S.H., Zhou, M.F., 2009. Geochemistry of the 430-Ma Jingbulake mafic–ultramafic intrusion in Western Xinjiang, NW China: implications for subduction related magmatism in the South Tianshan orogenic belt. Lithos 113, 259–273.

Yang, T.N., Li, J.Y., Sun, G.H., Wang, Y.B., 2006. Earlier Devonian active continental arc in Central Tianshan: evidence of geochemical analyses and Zircon SHRIMP dating on mylonitized granitic rock. Acta Petrologica Sinica 22, 41–48 (in Chinese with English abstract).

Yuan, C., Sun, M., Xiao, W.J., Li, X.H., Chen, H.L., Lin, S.F., Xia, X.P., Long, X.P., 2007. Accretionary orogenesis of the Chinese Altai: insights from Paleozoic granitoids. Chemical Geology 242, 22–39.

Yuan, C., Sun, M., Wilde, S., Xiao, W.J., Xu, Y.G., Long, X.P., Zhao, G.C., 2010. Post-collisional plutons in the Balikun area, East Chinese Tianshan: evolving magmatism in response to extension and slab break-off. Lithos 119, 269–288.

Zhai, W., Sun, X.M., Sun, W.D., Su, L.W., He, X.P., Wu, Y.L., 2009. Geology, geochemistry, and genesis of Axi: a Paleozoic low-sulfidation type epithermal gold deposit in Xinjiang, China. Ore Geology Reviews 36, 265–281.

Zhang, L.F., Ai, Y.L., Li, X.P., Rubatto, D., Song, B., Williams, S., Song, S.G., Ellis, D., Liou, J.G., 2007. Triassic collision of Western Tianshan orogenic belt, China: evidence from SHRIMP U–Pb dating of zircon from HP/UHP eclogitic rocks. Lithos 96, 266–280.

Zhang, Z.H., Wang, Z.L., Zuo, G.C., Liu, M., Wang, L.S., Wang, J.W., 2008. Age and tectonic setting of the volcanic rocks in Dabate ore district in West Tianshan Mountains and their constraints on porphyry-type mineralization. Acta Geologica Sinica 82, 1494–1503.

Zhang, D.Y., Zhang, Z.C., Xue, C.J., Zhao, Z.D., Liu, J.L., 2010a. Geochronology and geochemistry of the ore-forming porphyries in the Lailisigao'er-Lamasu Region of the Western Tianshan Mountains, Xinjiang, NW China: implications for petrogenesis, metallogenesis, and tectonic setting. Journal of Geology 118, 543–563.

Zhang, Z.H., Mao, J.W., Wang, Z.L., Pirajno, F., Wang, Y.B., 2010b. Geochemical and SHRIMP U–Pb age constraints on the origin of the Qingbulake mafic–ultramafic complex in the West Tianshan Mountains, Xinjiang, northwest China. Australian Journal of Earth Sciences 57, 819–837.

Zhao, Z.H., Xiong, X.L., Wang, Q., Wyman, D.A., Bao, Z.W., Bai, Z.H., Qiao, Y.L., 2008. Underplating-related adakites in Xinjiang Tianshan, China. Lithos 102, 374–391.

Zhao, Z.H., Xiong, X.L., Wang, Q., Bai, Z.H., Qiao, Y.L., 2009. Late Paleozoic underplating in North Xinjiang: evidence from shoshonites and adakites. Gondwana Research 16, 216–226.

Zheng, J.P., Griffin, W.L., O'Reilly, S.Y., Zhang, M., Liou, J.G., Pearson, N., 2006a. Granulite xenoliths and their zircons, Tuoyun, NW China: insight into SouthWestern Tianshan lower crust. Precambrian Research 145, 159–181.

Zheng, J.P., Griffin, W.L., O'Reilly, S.Y., Zhang, M., Liou, J.G., Pearson, N., Luo, Z.H., 2006b. The lithospheric mantle beneath the SouthWestern Tianshan area. Contribution to Mineralogy and Petrology 151, 457–479.

Zhou, M.F., Lesher, C.M., Yang, Z.X., Li, J.W., Sun, M., 2004. Geochemistry and petrogenesis of 270 Ma Ni–Cu-(PGE) sulfide-bearing mafic intrusions in the Huangshan district, Eastern Xinjiang, NorthWestern China: implications for the tectonic evolution of the Central Asian orogenic belt. Chemical Geology 209, 233–257.

Zhu, Y.F., Zhang, L.F., Gu, L.B., Guo, X., Zhou, J., 2005. SHRIMP geochronology and element geochemistry of Carboniferous volcanic rocks in the Western Tianshan area. Chinese Science Bulletin 50, 2004–2014.

Zhu, Z.X., Wang, K.Z., Xu, D., Su, Y.L., Wu, Y.M., 2006a. SHRIMP U–Pb dating of zircons from Carboniferous intrusive rocks on the active continental margin of Eren Habirga, West Tianshan, Xinjiang, China and its geological implications. Geological Bulletin of China 25, 986–991.

Zhu, Z.X., Wang, K.Z., Zheng, Y.J., 2006b. The Zircon SHRIMP dating of Silurian and Devonian granitic intrusions in the southern Yili Block, Xinjiang and preliminary discussion on their tectonic setting. Acta Petrologica Sinica 22, 1193–1200 (in Chinese with English abstract).

Zhu, Z.X., Li, J.Y., Dong, L.H., Zhang, X.F., Hu, J.W., Wang, K.Z., 2008a. The age determination of late Carboniferous intrusions in Mangqisu region and its constraints to the closure of oceanic basin in South Tianshan. Xinjiang. Acta Petrologica Sinica 24, 2761–2766 (in Chinese with English abstract).

Zhu, Z.X., Li, J.Y., Dong, L.H., Wang, K.Z., Liu, G.Z., Li, Y.P., Liu, Z.H., 2008b. Age determination and geological significance of Devonian granitic intrusion in Serikeyayilake region, northern margin of Tarim basin. Acta Petrologica Sinica 24, 971–976 (in Chinese with English abstract).

Zhu, Y.F., Guo, X., Song, B., Zhang, L.F., Gu, L., 2009. Petrology, Sr–Nd–Hf isotopic geochemistry and zircon chronology of the Late Paleozoic volcanic rocks in the southwestern Tianshan Mountains, Xinjiang, NW China. Journal of the Geological Society of London 166, 1085–1099.